AD-A087 745 DAVID W TAYLOR NAVAL SHIP RESEARCH AND DEVELOPMENT CE--ETC F/G 20/4
THEORETICAL CALCULATION OF VISCOUS-INVISCID TRANSONIC FLOWS.(U)
AUG 80 T C TAI

UNCLASSIFIED DTNSRDC/AERO-1268 DTNSRDC-80/104 NL

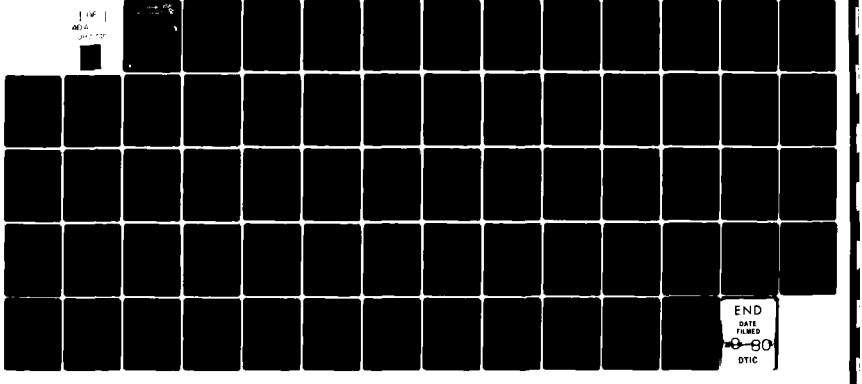

END
DATE FILMED
8-80
DTIC

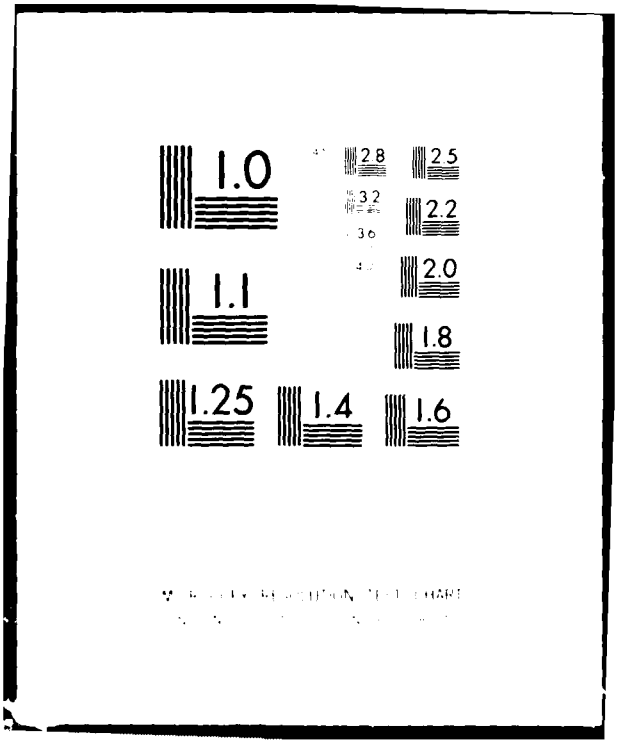
1.0
2.8
2.5
3.2
2.2
3.6
2.0
1.1
1.8
1.25
1.4
1.6

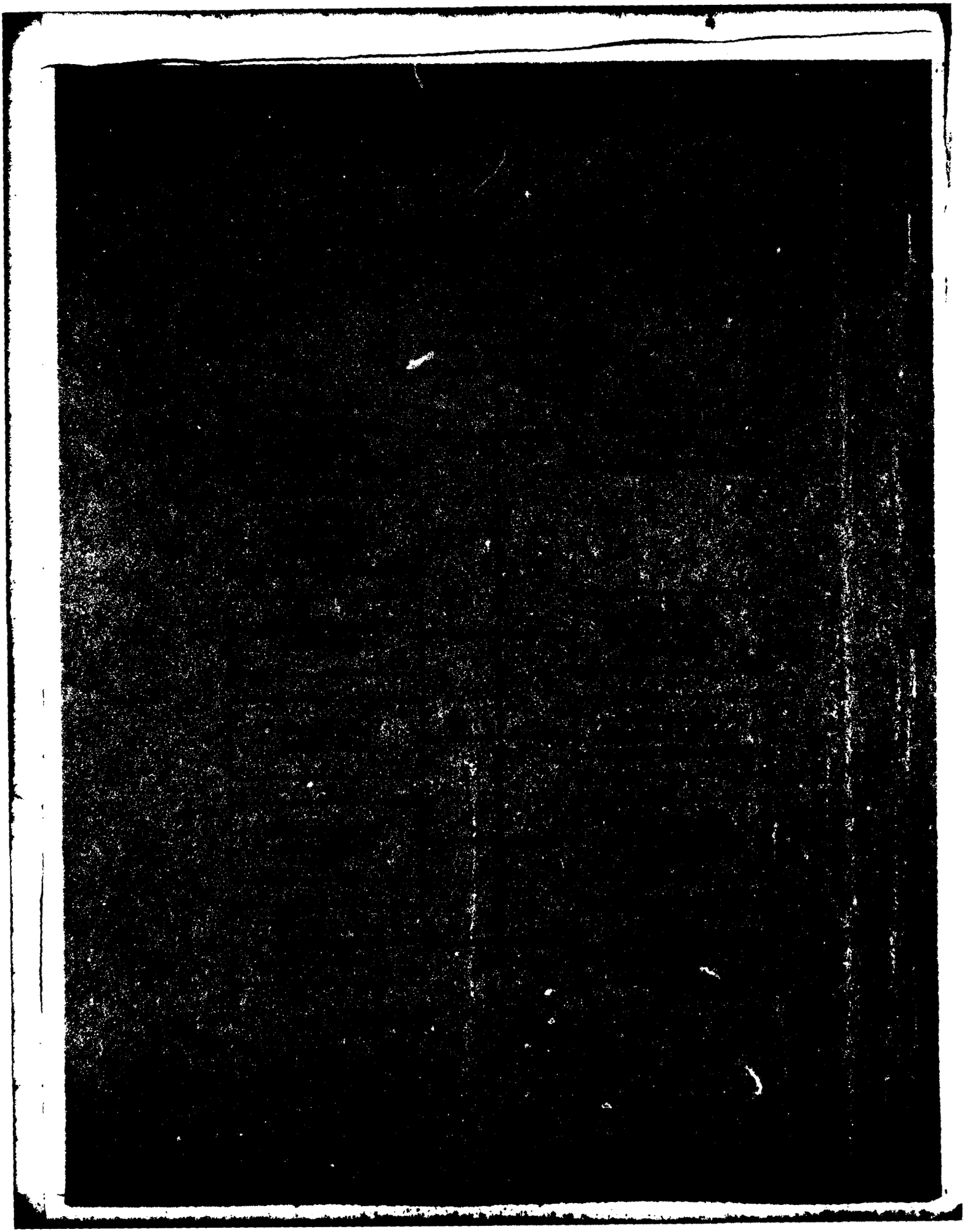

UNCLASSIFIED

SECURITY CLASSIFICATION OF THIS PAGE (When Data Entered)

REPORT DOCUMENTATION PAGE

READ INSTRUCTIONS BEFORE COMPLETING FORM

1 REPORT NUMBER: DTNSRDC/80/104	2. GOVT ACCESSION NO.: AD-A087745
3 RECIPIENT'S CATALOG NUMBER	
4 TITLE (and Subtitle): THEORETICAL CALCULATION OF VISCOUS-INVISCID TRANSONIC FLOWS	5. TYPE OF REPORT & PERIOD COVERED
6 PERFORMING ORG. REPORT NUMBER: Aero Report 1268	
7. AUTHOR(s): Tsze C. Tai	8. CONTRACT OR GRANT NUMBER(s): DTNSRDC
9. PERFORMING ORGANIZATION NAME AND ADDRESS: David W. Taylor Naval Ship Research and Development Center, Aviation and Surface Effects Department, Bethesda, Maryland 20084	10. PROGRAM ELEMENT, PROJECT, TASK AREA & WORK UNIT NUMBERS: (See reverse side)
11 CONTROLLING OFFICE NAME AND ADDRESS: David W. Taylor Naval Ship Research and Development Center, Technical Director, Bethesda, Maryland 20084	12. REPORT DATE: August 1980 13. NUMBER OF PAGES: 63
14 MONITORING AGENCY NAME & ADDRESS(if different from Controlling Office): Naval Air Systems Command, Code AIR-320D, Washington, D.C. 20361	15. SECURITY CLASS. (of this report): UNCLASSIFIED 15a. DECLASSIFICATION/DOWNGRADING SCHEDULE

16 DISTRIBUTION STATEMENT (of this Report)

APPROVED FOR PUBLIC RELEASE: DISTRIBUTION UNLIMITED

17. DISTRIBUTION STATEMENT (of the abstract entered in Block 20, if different from Report)

18 SUPPLEMENTARY NOTES

Presented at 1979-1980 Lecture Series on Shock-Boundary Layer Interaction in Turbomachines at the von Karman Institute for Fluid Dynamics, Belgium, 2-6 June 1980.

19 KEY WORDS (Continue on reverse side if necessary and identify by block number)

Transonic flows, viscous-inviscid interactions, integral boundary-layer method, strong interactions, weak interactions

20 ABSTRACT (Continue on reverse side if necessary and identify by block number)

The current status of computational capabilities for calculating viscous-inviscid transonic flows other than the solution of Navier-Stokes equations is presented. Techniques for solving transonic inviscid flows and compressible integral boundary layer methods are reviewed, and systems for strong viscous-inviscid interactions are described. Generally, the transonic viscous-inviscid interaction is characterized by a subcritical boundary layer with a supersonic outer stream. The thickening boundary layer produces a pressure rise which causes further thickening of the boundary layer. The physical flow is best modeled by direct coupling of the viscous

(Continued on reverse side)

DD FORM 1 JAN 73 1473 EDITION OF 1 NOV 65 IS OBSOLETE
S/N 0102-LF-014-6601

UNCLASSIFIED

SECURITY CLASSIFICATION OF THIS PAGE (When Data Entered)

(Block 10)

Program Elements 61152N, 61153N
Task Areas ZR-023-0201, WR-023-0201
Work Units 1606-105, 1606-300

(Block 20 continued)

and inviscid systems to allow immediate interaction between the shock wave and the boundary layer. It appears that the method of integral relations for the outer inviscid flow, combined with an integral boundary layer scheme, possesses such a capability. To facilitate the computation, an hybrid approach to the transonic inviscid solution, which consists of the finite difference method for solving the overall transonic inviscid potential flow field and the method of integral relations for solving Euler's equation in the shock region, is suggested. Finally, the application of the steady two-dimensional methods to the quasi two-dimensional problem on axisymmetric stream surface of a cascade flow at transonic speeds is discussed.

TABLE OF CONTENTS

LIST OF FIGURES

ABSTRACT

The current status of computational capabilities for calculating viscous-inviscid transonic flows other than the solution of Navier-Stokes equations is presented. Techniques for solving transonic inviscid flows and compressible integral boundary layer methods are reviewed, and systems for strong viscous-inviscid interactions are described. Generally, the transonic viscous-inviscid interaction is characterized by a subcritical boundary layer with a supersonic outer stream. The thickening boundary layer produces a pressure rise which causes further thickening of the boundary layer. The physical flow is best modeled by direct coupling of the viscous and inviscid systems to allow immediate interaction between the shock wave and the boundary layer. It appears that the method of integral relations for the outer inviscid flow, combined with an integral boundary layer scheme, possesses such a capability. To facilitate the computation, an hybrid approach to the transonic inviscid solution, which consists of the finite difference method for solving the overall transonic inviscid potential flow field and the method of integral relations for solving Euler's equation in the shock region, is suggested. Finally, the application of the steady two-dimensional methods to the quasi two-dimensional problem on axisymmetric stream surface of a cascade flow at transonic speeds is discussed.

ADMINISTRATIVE INFORMATION

The survey work presented in this report was supported by the Independent Research Program at the David W. Taylor Naval Ship Research and Development Center (DTNSRDC) under Work Unit 1606-105, and by the Naval Air Systems Command (AIR 320D) under AIRTASK 9R023-02-000, Work Unit 1606-300.

I. INTRODUCTION

Recent advances in numerical techniques have provided a powerful tool in transonic flow research. A complete full potential flow solution is now attainable in a matter of minutes by the finite difference relaxation scheme. Even a fully inviscid (nonisentropic) solution can be determined numerically by the unsteady finite difference approach at the cost of large computer time or by the method of integral relations with certain iterative procedures. The real transonic flow problem, however, is complicated by the viscous effect. The strong viscous-inviscid interaction caused by the shock wave thickens the boundary layer rapidly, and the flow eventually separates from the surface.[1-6] In such cases, the surface flow properties cannot be specified in advance, as in the usual formulation of boundary-layer theory, but are determined by interaction of the outer inviscid flow and the inner viscous flow near the surface. This has been referred to as the transonic viscous-inviscid interaction problem.

The problem of the viscous-inviscid interaction in the transonic region is complicated by the fact that the inviscid flow field is governed by mixed elliptic and hyperbolic partial differential equations for a compressible fluid flow. Because the major portion of the flow field is of the elliptic type, the velocity at the edge of the boundary layer at any location depends on the complete displacement thickness distribution. At the same time, the solution must satisfy the constraints characterized by the inviscid supercritical flow - the regularity condition at sonic points. The complete solution, therefore, involves tedious iterative procedures. Some advances in the area of laminar viscous-inviscid interactions at transonic speeds were made by MacCormack,[7] Klineberg and Steger,[8] Brilliant and Adamson,[9] and Tai.[10] Although the laminar flow yields an adequate model for assessing the basic mechanism of the strong viscous-inviscid interaction process, flows of practical interest at transonic speeds are turbulent because of high Reynolds number conditions. Theoretical treatment of the transonic turbulent viscous-inviscid interaction is further complicated by the turbulence. In the past several years, remarkable efforts have been devoted to the topic. The problem has been treated with various levels of assumptions.[11-18] In most cases, however, theoretical considerations were limited to weak shock conditions. The problem of strong viscous-inviscid interaction at transonic speeds was discussed by Klineberg and Steger,[8] and Tai.[10,15]

Generally, the problem of transonic viscous-inviscid interaction is best described by the Navier-Stokes equations. Because of extensive computer capacity requirements and other numerical problems, a complete Navier-Stokes solution for the subject problem still seems to be some time in the future.[19] Researchers will continue for many years to rely on other procedures to adequately account for the viscous effects. Among various techniques, the coupling of a valid transonic inviscid solution with an integral boundary-layer method seems to offer an adequate approach to the problem.

In the present paper, therefore, a review of both transonic inviscid solutions and the integral boundary-layer methods will be presented in Sections II and III. Because the review will not be exhaustive to cover such a field of phenomenal research activities, emphasis will be placed on prediction methods, either viscous or inviscid, which are adequate for handling the subject of

viscous-inviscid transonic flows. In Section IV, the problem of transonic viscous-inviscid interaction is described and calculation procedures are presented along with some theoretical results. Finally, the application of the methods developed for flows around airfoil to cascade flow problems is discussed.

II. REVIEW OF TRANSONIC INVISCID FLOW SOLUTIONS

Theoretical methods for solving the transonic inviscid flow have been advanced substantially in the past ten years. Because of the nonlinear nature of the flow equations, virtually all the solution procedures have been developed numerically. Solutions are achievable only with the aid of high speed computers.

1. BASIC FLOW EQUATIONS

The basic system of equations that govern an inviscid compressible fluid flow, without body force, is:

Continuity
$$\frac{\partial \rho}{\partial t} + \nabla \cdot \rho q = 0 \tag{1}$$

Momentum
$$\frac{Dq}{Dt} + \frac{1}{\rho}\nabla P = 0 \tag{2}$$

Entropy
$$T\frac{DS}{Dt} = \frac{De}{Dt} + P\frac{D}{Dt}\left(\frac{1}{\rho}\right) \tag{3}$$

where

ρ = static density, P = static pressure, q = velocity,
t = time, S = entropy, T = temperature,
e = internal energy.

Eq. (3) can be used to compute the rate of change of entropy of a fluid particle associated with the shock wave in a supercritical flow.

For regions prior to the shock wave and the far field, the changes of state of the fluid particle are isentropic

$$\frac{DS_1}{Dt} = 0 \quad \text{or} \quad S_1 = \text{Constant} \tag{4}$$

Instead of the energy equation, therefore, a simpler isentropic relation may be used

$$\frac{P}{P_o} = \left(\frac{\rho}{\rho_o}\right)^{\gamma} \tag{5}$$

For regions following the shock wave, where the fluid has a finite increase in entropy (or a decrease in the total pressure), the isentropic relation applies along a streamline

$$\frac{P}{P_o} = \left(\frac{\rho}{\rho_o}\right)^{\gamma} \exp\left(\frac{S_2 - S_1}{c_v}\right) \tag{6}$$

where subscripts 1 and 2 denote states before and after the shock wave, and o, the stagnation value. c_v is specific heat at constant volume.

The change of entropy $(S_2 - S_1)$ is normally small for transonic flows. However, because of the corresponding change of the downstream conditions, it may influence the location of the shock wave and thus alter considerable portions of the entire flow. Nonetheless, the flow behind the shock wave is still isentropic along a streamline. The new isentropic relation, however, must be based on a new entropy level which is slightly higher than its freestream value. The new entropy level differs from one streamline to another because the shock strength encountered on each streamline differs. Therefore,

$$S_2 \neq \text{Constant} \tag{7}$$

Because of the current status of numerical solutions for transonic viscous-inviscid interaction flows, the present paper will cover only two-dimensional, steady flow conditions. A brief discussion on the application to the unsteady, three-dimensional flow associated with turbomachinery will be given in Section V.

a. Full Inviscid Flow Equations

For two-dimensional, steady flows, the preceding system of equations reduce to the following form in Cartesian coordinates (x, y):

$$\frac{\partial(\rho U)}{\partial x} + \frac{\partial(\rho V)}{\partial y} = 0 \tag{8}$$

$$U\frac{\partial U}{\partial x} + V\frac{\partial U}{\partial y} = -\frac{1}{\rho}\frac{\partial P}{\partial x} \tag{9}$$

$$U \frac{\partial V}{\partial x} + V \frac{\partial V}{\partial y} = - \frac{1}{\rho} \frac{\partial P}{\partial y} \tag{10}$$

$$\frac{P}{P_o} = \left(\frac{\rho}{\rho_o}\right)^{\gamma} \exp\left(\frac{S_2 - S_1}{c_v}\right) \tag{11}$$

where U and V are velocity components and note that S_1 = constant and $S_2 \neq$ constant.

b. Full Potential Flow Equation

If the entire flow field is assumed isentropic, the flow is everywhere irrotational. The velocity is related to a potential function, Φ, as

$$U_i = \frac{\partial \Phi}{\partial x_i} = \text{grad } \Phi \tag{12}$$

The exact equation for the potential function for two-dimensional compressible flow can be written in Cartesian coordinates as

$$(a^2 - \Phi_x^2)\,\Phi_{xx} - 2\Phi_x \Phi_y \Phi_{xy} + (a^2 - \Phi_y^2)\,\Phi_{yy} = 0 \tag{13}$$

where

$$\Phi_x = \frac{\partial \Phi}{\partial x}, \quad \Phi_{xx} = \frac{\partial^2 \Phi}{\partial x^2}, \quad \Phi_{xy} = \frac{\partial^2 \Phi}{\partial x \partial y} \tag{14}$$

and a is the speed of sound. Eq. (13) is elliptic if the local Mach number $M < 1$ and hyperbolic if $M > 1$. Thus, Eq. (8) through (11) are reduced to a single differential equation, Eq. (13). Once the solution is found, the velocities are calculated from Eq. (12). Eq. (13) is valid only in cases with weak shock waves where the change of entropy can be neglected. By definition of the irrotational flow, there is no transonic wave drag.

c. Small Disturbance Equation

Further simplification of the equation system is to assume the perturbation velocities being small, resulting in the transonic small disturbance equation

$$(1 - M_\infty^2)\,\phi_{xx} + \phi_{yy} = \frac{M_\infty^2 (\gamma + 1)}{q_\infty}\,\phi_x \phi_{xx} \tag{15}$$

where ϕ is the perturbation potential function and other symbols have usual meaning.

The validity of this equation, of course, bears directly on the assumptions made, i.e., weak shock waves, thin airfoil at small angle of attack. And again, there is no transonic wave drag.

In all the foregoing systems, the viscosity is commonly neglected. The problem in coupling the viscous solution will be discussed later.

2. NUMERICAL SOLUTIONS

For convenience of discussion, numerical methods for the transonic inviscid problem can be classified into (a) finite difference method, (b) method of integral relations, (c) hybrid method, (d) finite element method, and (e) integral equation method. A brief review of these methods is presented below.

a. Finite Difference Method

The finite difference techniques for solving the transonic flow equation were introduced earlier by Emmons in 1948[20] using central differences in the subsonic region and upwind differencing in the supersonic zone. The technique was greatly improved by Murman and Cole[21] along with a successive line over-relaxation scheme. Through subsequent improvements in the area of different operators[22-24] and suitable and faster relaxation schemes,[25-28] the method has been highly developed for solving the full potential flow equations, as well as the transonic small-disturbance equations. Survey papers given by Yoshihara[29] and Bailey[30] summarizing early work in the use of the finite difference method and those of Jameson,[31] Murman,[32] and Ballhaus,[33] cover techniques implemented in the current widely used codes -such as those by Bauer et al.,[34] Jameson,[25] and Carlson.[35]

To illustrate the finite difference scheme in solving the transonic potential flow equation, a comprehensive discussion is given by Murman.[32] For simplicity, however, the approach is easily understood with reference to a Cartesian coordinate system. For this reason, the analysis developed by Carlson[35] using Cartesian coordinates is summarized below.

The full potential flow equation, Eq. (13), can be recast into the form of a perturbation potential ϕ

$$(a^2 - U^2)\phi_{xx} - 2UV\phi_{xy} + (a^2 - V^2)\phi_{yy} = 0 \tag{16}$$

where U and V are given by

$$\begin{aligned} U &= \Phi_x = q_\infty (\cos\alpha + \phi_x) \\ V &= \Phi_y = q_\infty (\sin\alpha + \phi_y) \end{aligned} \tag{17}$$

along with boundary conditions of velocity normal to the airfoil surface being zero and a velocity potential satisfying field behavior at infinity.

To incorporate the coordinate stretching in the physical plane and to avoid computational problems in the supersonic region, the potential flow equation is further arranged as

$$\left(1 - \frac{q^2}{a^2}\right)\phi_{SS} + \phi_{NN} = 0 \tag{18}$$

where

$$\phi_{SS} = \frac{1}{q^2}\left[U^2 f(f\phi_\xi)_\xi + 2UVfg\phi_{\xi\eta} + V^2 g(g\phi_\eta)_\eta\right]$$

$$\phi_{NN} = \frac{1}{q^2}\left[V^2 f(f\phi_\xi)_\xi - 2UVfg\phi_{\xi\eta} + U^2 g(g\phi_\eta)_\eta\right] \tag{19}$$

The S and N denote the vector parallel and perpendicular to the local velocity, respectively, and f and g are functions relating the Cartesian coordinates (x, y) and stretched coordinates (ξ, η), respectively, as

$$f = \frac{d\xi}{dx}, \quad g = \frac{d\eta}{dy} \tag{20}$$

The finite difference expressions with reference to a mesh system shown in Fig. 1 are, for example, for contributions to ϕ_{NN} when $q^2 > a^2$:

$$(f\phi_\xi)_\xi = \frac{1}{\Delta\xi^2}\left\{f_{i+\frac{1}{2}}(\phi_{i+1,j} - \phi_{ij}) - f_{i-\frac{1}{2}}(\phi^+_{ij} - \phi^+_{i-1,j})\right\} \tag{21}$$

For contributions to ϕ_{SS} when $q^2 > a^2$ and $V > 0$

$$(f\phi_\xi)_\xi = \frac{1}{\Delta\xi^2}\left\{f_{i-\frac{1}{2}}(\phi_{ij} - \phi_{i-1,j}) - f_{i-3/2}(\phi_{i-1,j} - \phi_{i-2,j})\right\} \tag{22}$$

These equations are so-called upwind difference formulas for supersonic points. For the subsonic region, a central differencing scheme is employed, for example,

$$(f\phi_\xi)_\xi = \frac{1}{\Delta\xi^2}\left\{f_{i+\frac{1}{2}}\,\phi_{i+1,j} - (f_{i+\frac{1}{2}} + f_{i-\frac{1}{2}})\left[\frac{\phi^+_{ij}}{w} + \left(1-\frac{1}{w}\right)\phi_{ij}\right] + f_{i-\frac{1}{2}}\,\phi^+_{i-1,j}\right\} \tag{23}$$

where the relaxation factor w has been incorporated into the difference formulas. When these expressions, Eqs. (21) through (23), are substituted appropriately into Eqs. (18) and (19) or Eq. (16), the result is a tridiagonal system of equations that can be solved for the current values of the function ϕ column i. Numerical stability is achieved by the incorporation of both old ϕ and new ϕ^+ values into the finite difference formula and the inclusion of time-like derivatives in the relaxation process. The result obtained by Carlson's code[35] is very close to that using the Jameson code,[25] see Fig. 2. Other applications of the finite difference method were reported elsewhere.[36,37]

An important feature in formulation of difference equations is the consistency condition with the original partial differential equations. Murman[22] discussed the topic in great detail and classified the difference equations for transonic flows into fully conservative form and not fully conservative form (or quasilinear form). Fig. 3 shows the difference in computed results using these two forms. It is observed that the nonconservative form yields a weaker shock wave but located slightly more upstream than that determined by the fully conservative equations. Murman has pointed out deficiencies in using the nonconservative formulas. Nonetheless, the nonconservative system is preferred by most users because of its better correlation with the experimental data. Tai[38] remarked that the momentum deficiency resulting from the nonconservative form has similar effects on the strength and location of the shock wave resulting from the total pressure deficiency aft the shock caused by the entropy rise across the shock wave. It will be further discussed in the next section.

b. Method of Integral Relations

The method of integral relations (MIR) provides another avenue to the solution of transonic flow problems. Previous applications of the method to transonic flows past airfoils include those by Holt and Masson,[39] Melnik and Ives,[40] Sato,[41] and Tai[42] for various flow conditions in the transonic regime. A review of the method in transonic flow is given by Holt.[43] The main advantage in using MIR is its ability to solve the full inviscid flow equations directly; thus the assumption of isentropic flow is not necessary.

In the numerical solution, it is convenient to write equations in nondimensional form normalized by freestream values. Therefore, the full inviscid flow equations, (Eqs. (8) through (11)), are recast as

Continuity
$$\frac{\partial (\rho U)}{\partial x} + \frac{\partial (\rho V)}{\partial y} = 0 \tag{24}$$

x–Momentum
$$\frac{\partial}{\partial x}(KP + \rho U^2) + \frac{\partial}{\partial y}(\rho UV) = 0 \tag{25}$$

y–Momentum
$$\frac{\partial}{\partial x}(\rho UV) + \frac{\partial}{\partial y}(KP + \rho V^2) = 0 \tag{26}$$

$$P = \rho^{\gamma} \exp\left(\frac{S_2 - S_1}{c_v}\right) \tag{27}$$

where
$$K = 1/(\gamma M_\infty^2).$$

The boundary conditions are as follows: at the airfoil surface, the normal velocity component equals to zero, i.e.,

$$q_n = 0$$

and at infinity, the flow is undisturbed, i.e.,

$$P = \rho = U = 1$$
$$V = 0$$

Briefly, in applying the system of flow equations must be written in divergence form

$$\frac{\partial}{\partial x} A(x, y, U, \ldots) + \frac{\partial}{\partial y} B(x, y, U, \ldots) = Q(x, y, U) \tag{28}$$

The divergence form of Eqs. (24) through (26) may then be integrated outward from the airfoil surface (but not necessarily normal to the surface) to each strip boundary successively at some x station. This procedure reduces the partial differential equations to ordinary ones. To perform the integration, the integrand is approximated by interpolation polynomials, for example A, by

$$A = \sum_{k=0}^{\bar{N}} a_k(x)(y - y_0)^k \tag{29}$$

where

$\bar{N}$ = the number of strips

$a_k(x)$ = constants evaluated at strip boundaries

y_o = the location of the base strip boundary.

In principle, the actual flow variation may be represented more closely by an increasing number of strips.

Using a basic second-order approximation for Eq. (29), the method can be implemented with up to five or six strips for desired accuracy. The process is illustrated in Fig. 4. The idea is to treat the whole integration domain as a series of different effective regions; a small number of strips may be used within each region. Three effective regions are designated by strip boundaries (0, 1, 2), (a, b, c), and (ξ, η, ζ). In each effective region, the flowfield is divided into two strips and approximated in the usual way by a second-order polynomial. The MIR is first applied to the boundaries ξ, η, ζ with the purpose of determining the shape of a streamline η and flow conditions along it. On the uppermost boundary ζ, freestream conditions are assumed to apply. Secondly, MIR is applied along boundaries a, b, and c to determine conditions along a streamline b, closer to the profile. Finally, MIR is applied in the disturbed part of the field along the boundaries 0, 1, and 2.

The resulting ordinary differential equations take on the form along boundaries a and b, for example

$$\frac{dU_a}{dx} = f_1(x, y, U_a, V_a, \ldots) \tag{30}$$

$$\frac{dV_a}{dx} = f_2(x, y, U_a, V_a, \ldots) \tag{31}$$

$$\frac{dU_b}{dx} = g_1(x, y, U_a, V_a, \ldots) \tag{32}$$

$$\frac{dV_b}{dx} = g_2(x, y, U_a, V_a, \ldots) \tag{33}$$

$$\rho_a = \left(\frac{C_s - U_a^2 - V_a^2}{C - 1}\right)^{\frac{1}{\gamma - 1}} \tag{34}$$

$$P_a = \rho_a^\gamma \exp\left(\frac{S_2 - S_1}{c_v}\right) \tag{35}$$

$$\rho_b = \left(\frac{C_s - U_b^2 - V_b^2}{C - 1}\right)^{\frac{1}{\gamma - 1}} \tag{36}$$

$$P_b = \rho_b^\gamma \exp\left(\frac{S_2 - S_1}{c_v}\right) \tag{37}$$

where

$$C = 1 + \frac{2}{(\gamma - 1)M_\infty^2}; \quad C_s = (C - 1)\frac{P_2}{\rho_2}$$

The set of Eqs. (31) through (34) are then solved by the fourth-order Runge-Kutta scheme. The solution is obtained by initial value techniques associated with a two-point boundary-value problem. For the flow over a lifting airfoil, the complete solution procedure consists of iterative processes for handling the regularity condition at the saddle point (sonic point), for determining the shock location and for enforcing the Kutta condition.

The method allows the exact Rankine-Hugoniot relations to be applied at the shock for determining the flow properties aft of the shock

$$\rho_2 = \rho_1 \frac{(\gamma + 1)M_1}{(\gamma - 1)M_1 + 2} \tag{38}$$

$$P_2 = P_1\left[1 + \frac{2\gamma(M_1^2 - 1)}{\gamma + 1}\right] \tag{39}$$

The change of entropy is obtained in terms of P_2 and ρ_2:

$$S_2 - S_1 = c_v \ln\left(\frac{P_2}{\rho_2^\gamma}\right) \tag{40}$$

where S_2 varies from one streamline to the other.

Figs. 5 and 6 show typical results obtained by the method of integral relations. These figures are taken from Tai[42] and include data from Magnus and Yoshihara,[44] Stivers,[45] Garabedian and Korn,[46] Krupp and Murman,[47] and Kacprzynski et al.[48] Reasonable agreements

between the theory and experiment were achieved except in the neighborhood of the shock wave. The disagreement there is attributed to a viscous-inviscid interaction between the shock wave and boundary layer. Note the effects of change of entropy (Fig. 5) and of the shock angle (Fig. 6) were explicitly evaluated. The increase in entropy corresponds to the decrease in total pressure.[49] Physically, the change of entropy creates vorticity behind the shock wave; it has a cumulative effect in the far downstream and consequently feeds back to the shock itself.[42] In the case of a finite increase in entropy across the shock wave, it was found that the shock strength was weakened and the shock location moved forward. It has a similar effect of the momentum deficiency of the nonconservative form in the finite difference method, although their mathematical bases are completely different.

c. Hybrid Method

The finite difference scheme and the method of integral relations for solving the transonic flow problems offer different kinds of advantages and disadvantages. The former is well developed, and easy for the user to implement; it is limited to the isentropic flow assumption (weak shock wave assumption)* and suffers mathematical inconsistency of the nonconservative formula. For the method of integral relations, on the contrary, the situation is opposite. It solves Euler's equation with a small computation requirement; but because of the multiple iterative processes involved, the whole solution procedure cannot be automated without man-machine interactions. To take advantage of the both and yet avoid their shortcomings, a hybrid method combination of the finite difference method and the method of integral relation appears to offer an unique capability for solving transonic flow problems with shock waves.

The central idea for the hybrid method proposed by Tai, is illustrated in Fig. 7. The overall mixed flowfield is governed by the potential flow equation except the shock region. In the shock region and the region downstream of the shock, the flow is governed by Euler's equation that allows entropy change, creating the transonic wave drag. First, the potential flow equation is solved by the finite difference relaxation procedure. The flow properties so calculated are valid up to the boundaries of the shock region marked by solid dots in Fig. 7. The values at these boundaries are then taken as the initial condition (those along the normal line) and the boundary condition (those along the streamwise line) for the numerical solution by the method of integral relations. In so doing, the major difficulty in treating the saddle point (sonic point) regularity condition associated with the method of integral relations is avoided and, therefore, in general, the procedure can be fully automated.

The concept is now being developed into a complete numerical procedure.

*The finite difference approach using Euler's equations has been developed using unsteady techniques[44] with extensive computer time and storage requirements.

d. Finite Element Method

The use of the finite element method in transonic flows is relatively new. A few references can be found in the literature.[50,51] Because of problems of hyperbolic behavior, the work has been limited to the small disturbance equations.

The following brief discussion of the method is taken from Chan and Brashears.[50]

In using the finite element method, the transonic small disturbance equation, Eq. (15), is rewritten as

$$\phi_{xx} + \phi_{yy} = f \tag{41}$$

where

$$f = \left[M_\infty^2 + M_\infty^2 (1+\gamma)\,\phi_x\right]\phi_{xx} \tag{42}$$

along with appropriate boundary conditions

$$q_n = 0 \qquad \text{on the airfoil}$$
$$\nabla\phi = 0 \qquad \text{at infinity}$$

Using Galerkin's weak form, Eq. (41) is then transformed to

$$\left[\iint N_i\,(N_{j,xx} + N_{j,yy})\,dxdy\right]\phi_j - \iint N_i\,f\,dxdy = 0 \tag{43}$$

In Eq. (43): N_i and N_j represent the shape functions, ϕ_j's are the unknown parameters, the indices i and j run from 1 to the total number of unknown parameters, and the integrations are to be performed over the entire domain under consideration.

Upon integrating by parts, there results

$$S_{ij}\,\phi_j = L_i \tag{44}$$

where

$$S_{ij} = \iint (N_{i,x}\,N_{j,x} + N_{i,y}\,N_{j,y})\,dxdy \tag{45}$$

and

$$L_i = \oint N_i \frac{\partial\phi}{\partial n}\,ds - \iint N_i \left[M_\infty^2 + M_\infty^2 (1+\gamma)\,N_{k,x}\,\phi_k\right] N_{\ell,xx}\,\phi_\ell\,dxdy \tag{46}$$

The original transonic problem is thus transformed into a system of algebraic equations in the form

$$S_{ij}\,\phi_j^{(n)} = L_i^{(n-1)} \tag{47}$$

where $\phi_j^{(n)}$ is the n^{th} step solution and $L^{(n-1)}$ is the load matrix evaluated by using the previous solution. Eq. (47) is to be solved subject to certain prescribed convergence criterion.

Fig. 8 shows a sample result of the finite element method for a supercritical flow past an NACA 64A006 airfoil; taken from Ref. 50. Using a triangular cubic element with 136 modes, the agreement between theory and experiment[52] is only qualitative. Generally, the method underpredicts the flow before the shock wave. Comparison between the finite element solution and the finite difference solution of a transonic flow is made by Hafez et al.,[51] as shown in Fig. 9. Again, the finite element method seems to underpredict the flow near the leading edge of the airfoil. Various ways for improving the finite element method in handing the mixed flow region and extension to the full potential flow equations have been discussed in Refs. 50 and 51.

e. Integral Equation Method

As opposed to the aforementioned methods, the integral equation method has been regarded as a seminumerical method in the sense that it employs analytical functions for representing the integrand. The integral equation was derived by Oswatitsch[53] thirty years ago for the solution of the transonic small-disturbance equation. The method was further explored by Gullstrand,[54] Spreiter and Alksne,[55] and Norstrud.[56] The integral equation method requires least numerical work. The disadvantage of the method is the difficulty in achieving an adequate field integral for approximating the complicated mixed flow field. Nixon[57,58] suggested that the accuracy of the integral equation method can be improved considerably by applying the field integral in regions of strips which divide the entire flow field. The accuracy of the integral can be increased simply by increasing the number of strips. The computational region can be, therefore, extended to "infinity" without introducing further numerical complexity. Fig. 10 shows some typical results obtained by using the extended integral equation method.[58]

III. REVIEW OF INTEGRAL BOUNDARY-LAYER METHODS

1. LAMINAR FLOWS

a. Laminar Boundary-Layer Equations

The governing equations for a compressible laminar boundary-layer flow in coordinates parallel and normal to the surface (s, n) are, with flow properties normalized by their freestream values.

Continuity

$$\frac{\partial (\rho u)}{\partial s} + \frac{\partial (\rho v)}{\partial n} = 0 \tag{48}$$

s–Momentum

$$\rho u \frac{\partial u}{\partial s} + \rho v \frac{\partial u}{\partial n} = - K \frac{dP}{ds} + \frac{1}{\rho_\infty V_\infty c} \frac{\partial}{\partial n} \left[\mu \frac{\partial u}{\partial n} \right] \tag{49}$$

where c is the chord length of an airfoil.

The boundary conditions are as follows: at the surface, $u = v = 0$; at the edge of the boundary layer, $u = U_e(s)$

b. Klineberg-Lees Method

The method was originally developed for analyzing the supersonic viscous-inviscid interaction problem.[59] Basically, the compressible flow equations, Eqs. (48) and (49) are transformed into an equivalent incompressible form by means of the Stewartson transformation.[60] The velocity profile based on an incompressible similarity solution can, therefore, be used in the integral approach. The resulting partial differential equations in a transformed incompressible plane, along with the equation for the rate of change of mechanical energy, i.e., the moment of momentum, are then integrated across the boundary layer from $n = 0$ to δ. In performing the integration, the parameter a is employed to denote the velocity profile for both attached and separated boundary layers. Profile quantities are then defined as functions of a.

The resulting ordinary differential equations are

$$\frac{d\delta_i^*}{ds} = F_1 (\delta_i^*, a, M_e) \tag{50}$$

$$\frac{da}{ds} = F_2 (\delta_i^*, a, M_e) \tag{51}$$

$$\frac{dM_e}{ds} = F_3(\delta_i^*, a, M_e) \tag{52}$$

where

δ_i^* = boundary layer displacement thickness
a = profile parameter
M_e = Mach number at the edge of boundary layer.

Functions F_1, F_2, and F_3 depend on variables δ_i^*, a, M_e and intermediate parameters H, J, Q, R, and Z, which have been defined as functions of a in Ref. 59. Curve-fitted polynomials, based on the similarity solution of the classical boundary-layer theory, are given in Ref. 59 for attached and separated flows, and in Ref. 61 for wake-reverse and wake-forward flows. The original ordinary system given by Ref. 59 has a temperature parameter. To simplify the discussion, it has been excluded in the above system for adiabatic flows.[10]

The basic features of the method are that (1) the boundary-layer properties depend on the variable a, which directly describes the velocity distribution, and (2) the velocity at the edge of the boundary layer is treated as a dependent variable, rather than a given quantity as in the conventional boundary-layer approach. The static pressure can, therefore, be determined by the interaction between the outer inviscid flow and the inner viscous layer near the surface. Such an arrangement allows direct coupling of the viscous system with inviscid equations for handling the viscous-inviscid interaction problem to be discussed later.

Fig. 11 shows the results of a typical computation for an adiabatic flow by the Klineberg-Lees method. The two solutions represent interactions beginning in the weak-interaction zone for both a finite and a semi-infinite flat plate. It is evident that a small change in the perturbation value can generate very different integral curves because of the high degree of nonlinearity of the equations in the subcritical region. The weak interaction solution corresponds to the conventional boundary-layer formulation, i.e., the M_e is "impressed" by the inviscid solution rather than calculated by the viscous-inviscid interaction. Note that the boundary-layer displacement thickness rises drastically due to the strong interaction.

2. TURBULENT FLOWS

a. Turbulent Boundary-Layer Equations

The governing equations for a compressible, adiabatic, turbulent boundary layer in coordinates parallel and normal to the surface (s, n) are with flow properties normalized by their freestream values.

Continuity

$$\frac{\partial (\rho u)}{\partial s} + \frac{\partial (\rho v)}{\partial n} = 0 \tag{53}$$

s-Momentum

$$\rho u \frac{\partial u}{\partial s} + \rho v \frac{\partial u}{\partial n} = - K \frac{dP}{ds} + \frac{1}{\rho_\infty V_\infty c} \frac{\partial}{\partial n}\left(\mu\beta \frac{\partial u}{\partial n}\right) \tag{54}$$

where β is an eddy viscosity parameter.

The boundary conditions are as follows: at the surface, $u = v = 0$. At the edge of the boundary layer, $u = U_e(s)$.

b. Kuhn-Nielsen Method

In the Kuhn-Nielsen method,[12] the above equations are transformed into incompressible plane (ξ, η) with the aid of the Stewartson transformation[60] along with the assumptions that the viscosity varies linearly with the temperature and that the Prandtl number equals unity. The velocity profile in the transformed plane used in performing the integration across the boundary layer is

$$\overline{u} = u_\tau \left[2.5 \ln(1 + \eta^+) + 5.1 - (3.39\eta^+ + 5.1)e^{-0.37\eta^+}\right] + 0.5\, u_\beta \left[1 - \cos\left(\pi \frac{\eta}{\delta}\right)\right] \tag{55}$$

where

u_β = wake velocity
u_τ = friction velocity
$\eta^+ = u_\tau \eta / \nu$

It is composed of an inner part, consisting of a laminar sublayer and the law-of-the-wall function, and an outer part, a wake function. It is a modification of Cole's law[62] with a laminar sublayer added.

The eddy viscosity model used in the Kuhn-Nielsen method is an extension of the two-layer model. For attached flow, the inner layer is represented by an expression given by Kleinstein.[63]

$$\beta = 1 + 0.0533\left\{e^{0.41\overline{u}/u_\tau} - \left[1 + 0.41\frac{\overline{u}}{u_\tau} + 0.5\left(0.41\frac{\overline{u}}{u_\tau}\right)^2\right]\right\} \tag{56}$$

In the outer layer, the Clauser expression along with an intermittency function of Klebanoff[64] is employed

$$\beta = \frac{0.013 + 0.0038\, e^{-(\delta^*/\tau_w)(dP/d\xi)/15}}{\left[1 + 5.5\left(\frac{\eta}{\delta}\right)^6\right]} \bar{u}_e \delta^* Re_\infty \tag{57}$$

For separated flow, the entire profile is based on a form given by Alber[65]

$$\beta = \frac{0.013\, \bar{u}_e \delta^* Re_\infty}{\left[1 + 5.5\left(\frac{\eta}{\delta}\right)^6\right]} \tag{58}$$

There results two ordinary differential equations

$$A_{11}\frac{du_\tau}{dx} + A_{12}\frac{d\delta}{dx} + A_{13}\frac{dU_e}{dx} = -\nu\, u_\tau |u_\tau| U_e \tag{59}$$

$$A_{21}\frac{du_\tau}{dx} + A_{22}\frac{d\delta}{dx} + A_{23}\frac{dU_e}{dx} = -\frac{\nu}{U_e \delta^2}\int_0^\delta \beta u_y dy \tag{60}$$

where A_{11} through A_{23} are defined in Ref. 12. The dependent variables are u_τ, δ, and U_e. In the computation, U_e is prescribed except in the region near separation, u_τ is prescribed, and U_e is calculated.

The results of a typical calculation for the flow over a bump at transonic speed are shown in Fig. 12. The viscous and inviscid solutions agree within one percent. For comparison, the measured δ^* and separation point are also shown. The calculated pressure is slightly higher than the experimental data.[66] The predicted δ^* is in excellent agreement with the data upstream of the shock wave. The theoretical δ^* for the converged strong interaction solution downstream of the shock is slightly lower than the experimented value probably due to the uncertainty in specifying the boundary-layer conditions downstream of the shock. More thorough analysis of the local shock-boundary layer interaction is needed to improve this aspect of the calculation and to handle the case of separation right at the shock.

c. Nash-Macdonald Method

The Nash-Macdonald method[67] is a semi-empirical formula for the solution of the momentum thickness, Θ, in the integral boundary-layer equation given by von Karman

$$\frac{d\Theta}{dx} = -(H + 2 - M_e^2)\frac{\Theta}{U_e}\frac{dU_e}{dx} + \frac{\tau_w}{\rho_e U_e^2} \tag{61a}$$

where the skin friction is determined by

$$\frac{\tau_w}{\rho_e U_e^2} = \left[F_c^{1/2}\left\{2.4711 \ln\left(F_R \frac{U_e\Theta}{\nu_e}\right) + 4.75\right\} + 1.5G + \frac{1724}{G^2 + 200} - 16.87\right]^{-2} \tag{61b}$$

Quantities F_c, F_R, and G are functions of the Mach number at the edge of boundary-layer and can be found in Ref. 67. The application of the method is straightforward. Some typical results are shown in Fig. 13 along with other theories[68-70] and experimental data.[71]

d. Stratford-Beavers Method

Similar to the foregoing method, semi-empirical formulas for calculating compressible turbulent boundary-layers were developed by Stratford and Beavers.[72] The formulas for the momentum and the boundary-layer displacement thickness are
For freestream Reynolds numbers of the order of 10^6,

$$\theta = 0.036\left(1 + \frac{M_e^2}{10}\right)^{-0.7} s\, Re_s^{-1/5}$$
$$\delta^* = 0.046\left(1 + 0.8M_e^2\right)^{0.44} s\, Re_s^{-1/5} \tag{62}$$

For freestream Reynolds numbers of the order of 10^7,

$$\theta = 0.022\left(1 + \frac{M_e^2}{10}\right)^{-0.7} s\, Re_s^{-1/6}$$
$$\delta^* = 0.028\left(1 + 0.8M_e^2\right)^{0.44} s\, Re_s^{-1/6} \tag{63}$$

where

$$s = \frac{1}{W}\int_0^x W\, d\xi \tag{64}$$

$$W = \left(\frac{M_e}{1 + 0.2M_e^2}\right)^4 \tag{65}$$

$$Re_s = \frac{s\,U_c}{\nu} = \frac{a_o}{\nu_o}\frac{s\,M_e}{(1 + 0.2M_e^2)^{3-\omega}} \tag{66}$$

The suffix o refers to stagnation. The quantity w is the exponent in the viscosity-temperature relation $\mu \propto T^{\omega}$, a reasonable value for ω being 0.75, except at very high temperatures, where $\omega = 0.5$.

The results of the shape factor δ^*/θ found by Eqs. (62) and (63) compare fairly closely to that of a $1/n^{th}$ power law, where n = 7 and 9 (see Fig. 14).

IV. TRANSONIC VISCOUS-INVISCID INTERACTIONS

1. DESCRIPTION OF VISCOUS-INVISCID TRANSONIC FLOWS

The schematic of the transonic viscous-inviscid interaction over an airfoil surface is represented in Fig. 15. The embedded supersonic region of a supercritical flow has to be terminated by a shock wave to bring the downstream flow back to the subsonic state, and the shock foot is smeared into a series of compression waves as a result of viscous-inviscid interactions. The presence of an adverse pressure gradient due to the compression before the shock usually causes the boundary layer to separate from the surface for either laminar or turbulent boundary layers. However, the flow behavior near the shock differs considerably, depending on whether the boundary layer is laminar or turbulent ahead of the point where it meets the shock.[3] The pressure rises more rapidly for turbulent than for laminar layers,[3,4] while the displacement thickness of the boundary layer increases considerably through the shock, more so for laminar than for turbulent layers.[2] Reynolds number has a strong effect on the interaction in the case of laminar boundary layers but almost no effect for turbulent flows.[2,4] In any event, the basic features of boundary-layer thickening and pressure rising are common for both layers.

Beyond the separation point, the boundary-layer flow is divided into two regions by the dividing streamline.[73-75] The flow above this streamline includes all the fluid contained in the boundary layer just upstream of separation. Below this streamline, the flow yields a separated pattern with reversed profile near the wall. Two kinds of separated-flow pattern have been observed by Pearcey et al.[5] for turbulent boundary layers. One deals with a local separation bubble caused by the shock; the other is involved with rear separation and depends on the magnitude of

the pressure gradient approaching the trailing edge and on the upstream history of the boundary layer.

The pressure rises continuously in the subsonic portion although its gradient decreases steadily after the toe of the shock.[5] This feature differs from that of a supersonic free interaction in which the incident shock is reflected as an expansion fan which turns the flow toward the surface and thus enables the reattachment of the boundary layer. In the transonic case, however, the shock is an embedded one which serves as part of the compression process of the flow over the rear of the airfoil; whereas, the boundary layer, especially the laminar one, does not have sufficient energy for reattachment against continuous adverse pressure gradients and, therefore, remains separated all the way toward the trailing edge (see Fig. 16).

The mechanism of turbulent viscous-inviscid interaction differs from that of laminar interaction. In the turbulent case, when the flow enters the strong interaction zone, it turns away from the surface in response to a rapid separation bubble growth, triggered from the toe of the shock; see Ref. 5. For the latter case, the compression before the shock is fairly long and smooth and involves no rapid change in the flow angle at the edge of the boundary layer; see Fig. 17.

2. STRONG VERSUS WEAK INTERACTION FORMULATIONS

In analysis of viscous transonic flows, it is necessary for the analytical model of the viscous system to have the capability for allowing communication of positive pressure disturbance from the embedded shock wave upstream through the subsonic portion of the boundary layer. The surface pressure should be calculated by the viscous equations rather than specified by the inviscid system. The communication of the pressure disturbance through the viscous layer becomes possible because of the direct influence between the pressure and boundary layer thickness in a subcritical boundary layer. At local supersonic speeds, a thickening subcritical boundary layer produces a rise in pressure in the outer stream which causes further thickening of the boundary layer.[59]

The viscous system is linked to the inviscid system through a common variable by which the change of flow properties of the outer flow may be transmitted to the inner flow or vice versa. It reflects the physical phenomenon of the shock wave/boundary-layer interaction process wherein there is a steep pressure rise before the arrival of the shock wave because of the influence exerted by the shock. This concept of the new viscous system has been explored in supersonic flows by Klineberg and Lees[59] and Lees and Reeves[73] and in transonic flows by Klineberg and Steger,[8] and Tai.[10,15]

The new system model is referred to as the strong interaction formulation. Other formulations, such as the usual boundary-layer system by which the viscous effect is accounted for by the displacement correction or analytical techniques which do not involve flow separation, are referred to as the weak interaction. The strong interaction formulation may be applied to attached, as well as separated, boundary layers. When applied to attached flows, the boundary layer eventually separates. If the same flow were to be treated by the weak interaction system,

numerical experiments indicate that the boundary layer would remain attached until shock jump was encountered. This gives further indication that the strong interaction system is more suitable in simulating the shock wave boundary-layer interaction process than are the usual boundary-layer approaches. On the other hand, the use of weak interaction formulation is preferred in the forward portion of the airfoil where the viscous-inviscid interaction is presumably weak.

3. CALCULATION OF WEAK INTERACTIONS

a. Boundary Layer Correction

As in the usual procedure, the boundary-layer quantities are calculated based on the specified inviscid pressure distribution, and the inviscid solution is updated based on the surface augmented by the boundary-layer displacement thickness.* In so doing, the two flows are connected at the locus of the boundary-layer displacement thickness. The latter serves as a "streamline" through which mass transfer or more importantly, direct communication between the outer inviscid and inner boundary-layer flows is prohibited. The inviscid solution is then repeated until a converged solution is obtained upon satisfying converging criterion after several iterations.

Existing transonic codes by Bauer et al.,[34] and Carlson[35] determine the viscous effects by such a procedure. The Nash-Macdonald method[67] for turbulent boundary layers is used in both codes (weak interaction in the laminar case is simply neglected). In the case of transonic cascade flows, Gliebe coupled an inviscid flow solution by a finite-difference method and a viscous flow solution by the Stratford-Beavers method.[72] Fig. 18 shows typical results of the boundary-layer effect on the blade of a cascade flow evaluated by Gliebe.[18]

b. Analytical Method

Mason and Inger[14] have developed an analytical method for calculating the transonic viscous-inviscid interaction involving a weak normal shock wave impinging on unseparated turbulent boundary layers. The interaction field is considered as a multisubregion problem and the resulting viscous transonic flow system is solved by the Fourier transformation method. The theoretical model is valid for weak shock conditions with the Mach number ahead of the shock not very near unity. The schematic of the model which is shown in Fig. 19 includes outer mixed flow and inner rotational disturbance flow with a Lighthill sublayer.

c. Asymptotic Expansion Method

Melnik and Grossman,[13] on the other hand, formulated an asymptotic expansion method for analyzing the interaction of a normal shock wave with an unseparated turbulent boundary

*Another way of accounting for the boundary-layer effect is to determine an equivalent source distribution $\sigma = d(U_e\delta^*)/ds$ as suggested by Lighthill.[76]

layer on a flat surface at transonic speeds. The interaction involves an outer, inviscid rotational layer, a constant shear stress layer near the wall, and a blended layer between the two. Fig. 20 shows typical results of the asymptotic method compared with those of the Manson-Inger scheme.[14]

4. CALCULATION OF STRONG INTERACTIONS

a. Laminar Viscous-Inviscid Interaction

The calculation is illustrated by using the integral boundary layer method coupled with an inviscid solution by the method of integral relations.[10] The coordinate system for the coupling is shown in Fig. 21. The ordinary differential equations for the inviscid external flow, reduced by the method of integral relations, are (for simplicity only those at the edge of the boundary layer are written here)

$$\frac{dU_e}{dx} = f_1 \qquad (30)\text{bis}$$

$$\frac{dV_e}{dx} = f_2 \qquad (31)\text{bis}$$

and those for the viscous system[10] are

$$\frac{d\delta_i^*}{ds} = F_1 \qquad (50)\text{bis}$$

$$\frac{da}{ds} = F_2 \qquad (51)\text{bis}$$

$$\frac{dM_e}{ds} = F_3 \qquad (52)\text{bis}$$

The viscous system is coupled directly to the inviscid system by the induced angle of inviscid streamline at the edge of the boundary layer

$$\Theta = \sin^{-1}\left[\frac{V_e\ (\text{invis.})}{M_e a_e\ (\text{viscous})}\right] \qquad (67)$$

where V_e is calculated by the inviscid system, while the velocity magnitude $M_e a_e$ is obtained by the viscous system. The variable Θ is a common variable for both inviscid and viscous systems and, therefore, governs the viscous-inviscid interaction process. Since the two flows are coupled

by the inviscid streamline angle rather than the streamline itself, mass transfer between the outer inviscid and inner boundary-layer flows is allowed in accordance with the continuity equations by which the variable Θ is introduced in the viscous system

$$\frac{d\delta^*}{ds} = \tan\Theta + (\delta - \delta^*)\frac{d}{ds}\left[\ln(\rho_e U_e)\right] \tag{68}$$

The value of Θ, which is determined by the viscous-inviscid interaction, has a direct bearing on the growth of the boundary layer.

The strong interaction system is applied at some distance preceding the inviscid shock location. The exact initial location of the strong interaction region is determined by an iterative process.[10]

Results of calculations at supercritical freestream Mach numbers are presented for both a 6 percent circular arc and an NACA 0015 airfoil.

Fig. 22 gives the boundary-layer displacement thickness throughout a 6 percent circular arc airfoil at $M_\infty = 0.868$ and $Re_\infty = 6.9 \times 10^4$. The thickening of the boundary layer in the forward portion follows a similar trend as that found by Schubauer, using the Karman-Polhausen method[77]; however, the strong interaction calculation gives a far more realistic δ distribution pattern in the rear portion. The boundary layer is practically of the Blasius type ($a = 1.857$) in the leading-edge region and varies slightly throughout the forward portion of the airfoil. It remains unseparated through the embedded supersonic region although the viscous-inviscid interaction has been strong since $x = 0.37$. The separation point is found when $a = 0$ which corresponds to zero shearing stress at the wall.

The boundary layer keeps separated over the rear of the airfoil where small adverse pressure gradients are generated by continuous compression of the outer subsonic flow. This is a physical feature of the transonic viscous-inviscid interaction since by compression, the flow ought to return almost to the freestream value downstream. After leaving the trailing edge, the viscous wake contains a reversed flow for a distance and then turns to forward flow downstream. The location of the rear stagnation point agrees well with that found by Klineberg and Steger[8] under similar flow conditions.

Theoretical results of pressure distribution for the 6 percent circular arc airfoil compare very well with recent laminar experimental data of Collins and Krupp[78] as presented in Fig. 23, not only in the pressure distribution but also in the separation point. The small difference in freestream Mach number between theory and experiment was deliberately selected to offset wind-tunnel interference effects.[79] Fig. 23 also shows the inviscid isentropic and nonisentropic solutions obtained by using the method of integral relations with three different shock conditions. Note that the shock foot is smeared as a result of the strong viscous-inviscid interaction. The inviscid result with $\Delta S > 0$ and $\beta = 75$ degrees simulates the flow best in the region near the shock; however, it still deviates from the viscous data in the trailing edge. The difference is obviously attributable to the thickening of the laminar boundary layer toward the trailing edge.

On the other hand, comparisons between theory and experiment for the NASA 0015 airfoil were jeopardized because of lack of available laminar test data. Measurements available for this case were taken from Graham et al.[80] at Reynolds numbers on the order of 2×10^6; the flows were, therefore, turbulent. The calculated laminar result is in good agreement with the experimental data in the forward portion of the airfoil; however, there is considerable discrepancy in pressure near the trailing edge; see Fig. 24. The deviation may be attributed to the extended separation of the laminar boundary layer, which would be unlikely to occur if the boundary layer were turbulent. Since the method of using reversed-flow velocity profile was originally attempted for application to cases with small adverse pressure gradients[81], this discrepancy also raised questions regarding the validity of its use in separated boundary layers with strong adverse pressure gradients.

Finally, Fig. 25 shows the overall flowfield of the NACA 0015 airfoil at $M_\infty = 0.729$, $\alpha = 4$ degrees, and $Re_\infty = 0.145 \times 10^6$, based on the chord length. The calculated boundary layer is fairly thin because of the high Reynolds number used. The separated boundary layer on the lower side is thicker than that on the upper side because the latter is developed from a very thin attached layer in an accelerating external flow prior to the shock wave. In any case, the basic features of the transonic viscous-inviscid interaction are clearly seen. The compression waves in the region near the shock are represented by the Mach lines. Being normal to the edge of the boundary layer, the Mach one line represents the end of a smearing shock toe rather than the whole shock. The mechanism of the compression has been designated in the literature as the "lambda shock," which serves as part of the decelerating process of the flow over the rear of the airfoil, where the laminar boundary layer does not have sufficient energy for reattachment against continuous adverse pressure gradients and, therefore, remains separated all the way to the trailing edge.

It is also interesting to note that the viscous-inviscid interaction process terminates the embedded supersonic flow earlier than does the inviscid shock. The result is not surprising since the interaction process has weakened the strength of the shock wave; in turn, it moves the shock forward.[42,82] However, because of the change of the local velocity distribution, the height of the supersonic pocket determined by the theory is slightly higher than that obtained by the inviscid solution; it remains to be verified by appropriate experiment and other valid analysis.

The integral boundary layer method can also be coupled with a finite difference scheme carried out by Klineberg and Steger.[8] There the V_e values were prescribed rather than calculated. Although the prescribed V_e values were improved successively, the viscous and inviscid flows had to be treated separately even for the strong interaction. More importantly, in the indirect coupling as such, it would be difficult to allow direct communication, including the mass transfer, between the outer inviscid flow and the boundary layer flow.

b. Turbulent Viscous-Inviscid Interaction

Because of the convenience for direct coupling of the outer inviscid and viscous flows, the method of integral relation is used again for the inviscid solution in the illustration for calculating the turbulent viscous-inviscid interaction.[15] The coordinate system and inviscid flow equations are the same as for the laminar case; Eqs. (30) and (31). The equations for the viscous system are derived by adding the continuity equation to the original Kuhn-Nielsen method,[12] i.e.,

$$\frac{d}{d\xi}\int_0^{\delta}\bar{u}d\eta - \bar{u}_e\frac{d\delta}{d\xi} = -\bar{v}_e \tag{69}$$

The resulting viscous system is[15]

$$\begin{bmatrix} E_{11} & E_{12} & E_{13} \\ E_{21} & E_{22} & E_{23} \\ E_{31} & E_{32} & E_{33} \end{bmatrix} \begin{bmatrix} \frac{du_\tau}{d\xi} \\ \frac{d\delta}{d\xi} \\ \frac{du_e}{d\xi} \end{bmatrix} = \begin{bmatrix} Q_1 \\ Q_2 \\ Q_3 \end{bmatrix} \tag{70}$$

where E_{ij} and Q_j are presented in Ref. 15. The system is valid for both attached and separated flows.

Similar to the laminar analysis,[10] the viscous system is coupled directly to the inviscid system by the induced angle of the inviscid streamline at the edge of the boundary layer, which allows mass transfer between the two flows in accordance with the continuity equation, Eq. (69). The strong interaction system is applied at some distance before the inviscid shock wave location. As opposed to the laminar case, the flow angle at the edge of the boundary layer is adjusted. The reason for the adjustment is that in the turbulent case, when the flow enters the strong interaction zone, it turns away from the surface in response to a rapid separation bubble growth, triggered from the toe of the shock; see Ref. 5. The boundary layer is attached at the start of the strong interaction region; however, it usually separates in a short distance. Computation is then switched to the subroutines based on separated velocity profiles of the strong interaction system.

Results of calculations at supercritical freestream Mach numbers are presented for a 10-percent thickness bump and an NACA 0015 airfoil at an angle of attack. The bump is basically a 10-percent circular arc, faired with cosine curves at both ends. Fig. 26 gives the typical velocity profile at different stations over the 10-percent thickness bump at $M_\infty = 0.7325$ and $Re_\infty = 1.75 \times 10^6$. The profile at $x = 0.2$ is the initial profile, calculated by using Schlichting's skin friction

formula based on a power law distribution.[83] Good comparison between the calculated and available measured profiles of Alber et al.[66] at x = 0.5 and 0.875 indicates the adequacy of the theoretical approach.

Fig. 27 shows the distribution of the friction velocity over the same bump. Note that the friction velocity in the strong interaction region is calculated in the analysis, rather than prescribed as in Ref. 12. The flow separates in a fairly short distance after it enters the strong interaction zone influenced by the shock. The friction velocity remains almost constant downstream of the separation point and then increases gradually toward reattachment. The calculated pressure distribution compares fairly well with recent turbulent experimental data of Alber et al.[66] as presented in Fig. 28. Also plotted are the inviscid solutions obtained by using the method of integral relations, with and without entropy change across the shock. The agreement between theoretical and experimental results is good both for pressure distribution and separation point. Note that the shock foot is smeared as a result of the strong viscous-inviscid interaction. The compression starts at x = 0.575 where the strong interaction begins. The turbulent boundary layer is attached throughout the supersonic region and the strong interaction starts in front of the shock wave. Flow separation takes place downstream of the shock wave at a peak Mach number of 1.14. The trend is consistent with that found experimentally by Alber et al.[66] for cases with $M_p < 1.32$. The turbulent boundary layer reattaches downstream of the bump. The difference between the theoretical and experimental pressures in the rear of the bump is attributed to the insufficient damping effect in the inner layer eddy viscosity model. There is also reason to believe that it may be due to overprediction of the flow by the strong interaction equations.

The flow over an NACA 0015 airfoil at $M_\infty = 0.729$ and $\alpha = 4$ degrees has been investigated as an example for the lifting case. This particular flow condition has been calculated in the laminar analysis.[10] There the agreement between the laminar theory and the experiment was good except in the rear of the airfoil, where the flow could have become turbulent. Therefore, the turbulent viscous-inviscid interaction model is employed for flows in the rear portion of the airfoil. The transition zone is assumed to be short enough so that the continuity of boundary layer properties may be maintained. The corresponding initial turbulent shear velocity is then estimated based on similar velocity profiles for both laminar and turbulent boundary layers. The weak interaction system is used in actual computation after the strong interaction formulation fails to produce a converged solution. Calculated results are given in Fig. 29 along with the previous laminar solution[10] and the experimental data of Graham et al.[80]

As indicated in Fig. 29, the pressure values over the rear region of the airfoil calculated by the present turbulent theory compare fairly well with the experimental data, Ref. 80, which were measured at Reynolds numbers on the order of 2×10^6. The flow over the upper surface has undergone a strong viscous-inviscid interaction in the vicinity of the shock wave between x = 0.34 and 0.6, but it seems to have returned to a weak interaction process after x = 0.6; even the boundary layer is still separated thereafter. The boundary layer remains separated all the way to the trailing edge. It follows a similar flow pattern to that observed by Pearcey et al.[5]

5. VISCOUS-INVISCID INTERACTION IN SEPARATED FLOW REGION

Although the strong interaction formulation is useful and necessary for the shock wave region, it suffers a problem of accuracy and numerical stability in the separated flow region. The reason for this is believed to be attributed to the basic feature of the strong interaction system that the pressure is calculated simultaneously with the boundary layer thickness. The results of the integral methods are therefore, much more sensitive to the velocity profiles used for either laminar or turbulent boundary layers. Any inadequacies in velocity profiles employed will be magnified in the strong interaction system, as opposed to being suppressed in the usual boundary layer calculations.

In general, the velocity profiles for separated flows are more difficult to define than for attached boundary layers. In the foregoing laminar case, the reversed-flow profile was originally attempted for application to cases with small adverse pressure gradients.[81] Its use in separated boundary layers with strong adverse pressure gradients introduced some discrepancy in agreement between the theory and the experiment in the trailing edge region.[10]

In the case of turbulent flows, on the other hand, a numerical difficulty is encountered in using the strong interaction system. Very fine adjustment of friction velocity u_τ has to be made for achieving the convergence of the flow downstream of the separation point,[15] see Fig. 30. Because of the convergence problem, it is proper to use the weak interaction system (pressure prescribed) rather than the strong interaction formulation near and aft the separation point.

These arguments suggest that in the separated flow region, a weak interaction system might provide more reliable results than the strong interaction formulation. The point of switching from the strong to the weak interaction equations has to be determined by numerical experiments.

V. APPLICATION TO CASCADE FLOWS

The flow in a cascade at transonic speeds is far more complex than the steady, two-dimensional flow past an airfoil in free air. A comprehensive review of the flow in transonic compressors has been given by Kerrebrock.[84] To apply the previous techniques to cascade flows involving transonic viscous-inviscid interactions, assumptions that are necessary are that the flow in a cascade has axisymmetric stream surfaces and that the flow on these surfaces can be treated two dimensionally. Such flows very nearly exist in cascades where the blade height is small compared to the radius from the centerline of the cascade. They are called quasi two-dimensional flows.[85] The schematic of a quasi two-dimensional flow in an axisymmetric stream surface is depicted in Fig. 31. The approximation represents an idealized situation for the complex unsteady flow in transonic compressors. It is, nevertheless, useful for qualitative investigation of the influence of various design parameters.

The governing equation for a quasi two-dimensional compressible inviscid flow in an axisymmetric stream surface represented by coordinates (ξ, θ) is[85]

$$\frac{1}{hR}\frac{\partial}{\partial\theta}\left(\frac{1}{\rho}\frac{\partial\psi}{\partial\theta}\right) + R\frac{\partial}{\partial\xi}\left(\frac{1}{h\rho}\frac{\partial\psi}{\partial\xi}\right) + \frac{\partial R}{\partial\xi}\frac{1}{h\rho}\frac{\partial\psi}{\partial\xi} = -2\omega R\frac{\partial R}{\partial\xi} \tag{71}$$

where

ω = constant rotation of the cascade
R = distance measured from the axis
h = blade height

The stream function ψ is defined by

$$\frac{\partial\psi}{\partial\xi} = \rho hV \tag{72}$$

$$\frac{\partial\psi}{\partial\theta} = -\rho hRU$$

The boundary conditions are $q_n = 0$ on the blade surfaces.

Eq. (71) can be solved by the finite difference-relaxation method, similar to the procedure employed in a two-dimensional potential flow about an airfoil.

To facilitate calculating the strong viscous-inviscid interactions and to account for the non-isentropic effect of the embedded shock, it was suggested in the foregoing discussions that the hybrid method is mostly suitable for the purpose. That is, the flow in the shock region is solved by the method of integral relations with the initial and boundary conditions provided by the finite difference-relaxation approach. To implement the method of integral relations, the governing equations for the quasi two-dimensional channel flow between the cascade blade surfaces are written in primitive form as

Continuity
$$\frac{\partial(\rho U)}{\partial\xi} + \frac{\partial(\rho V)}{R\partial\theta} = -\frac{\rho U}{Rh}\frac{d(Rh)}{d\xi} \tag{73}$$

ξ-Momentum
$$\frac{\partial(\rho U^2 + P)}{\partial\xi} + \frac{\partial(\rho UV)}{R\partial\theta} = -\frac{\rho U^2}{Rh}\frac{d(Rh)}{d\xi} + \rho(V + \omega R)^2\frac{1}{R}\frac{dR}{d\xi} \tag{74}$$

θ-Momentum
$$\frac{\partial(\rho UV)}{\partial\xi} + \frac{\partial(\rho V^2 + P)}{R\partial\theta} = -\frac{\rho UV}{Rh}\frac{d(Rh)}{d\xi} - \rho U\left(\frac{V}{R} + 2\omega\right)\frac{dh}{d\xi} \tag{75}$$

Entropy

$$\frac{P}{P_o} = \left(\frac{\rho}{\rho_o}\right)^{\gamma} \exp\left(\frac{S_2 - S_1}{c_v}\right) \tag{76}$$

With a boundary condition of zero normal velocity on the surface, Eqs. (73) through (76) can be solved by the method of integral relations with the aid of the N-2-strip scheme.[42] The final solution is achieved by updating solutions between the finite difference method for the overall flow and the method of integral relations for the shock region.

The inviscid solution so obtained is convenient to be coupled with either laminar or turbulent viscous systems for strong interaction between the shock wave and the boundary layer. A weak interaction formulation should be applied for conventional boundary layer regions, including a separated flow zone downstream of the shock wave.

VI. REFERENCES

1. Liepmann, H.W., "Interaction between Boundary Layers and Shock Waves in Transonic Flow," Journal of the Aeronautical Sciences, Vol. 13, pp. 223–237 (Dec 1946).

2. Ackeret, J., Feldmann, F., and Rott, N., "Investigations of Compression Shocks and Boundary Layers in Gases Moving at High Speeds," NACA TM 1113 (Jan 1947).

3. Holder, D.W., Pearcey, H.H., and Gadd, G.W., "The Interaction between Shock Waves and Boundary Layers," Aeronautical Research Council, London, England, CP 180 (Feb 1954).

4. Holder, D.W., "The Transonic Flow Past Two-Dimensional Aerofoils," Journal of the Royal Aeronautical Society, Vol. 68, pp. 501–516 (Aug 1964).

5. Pearcey, H.H., Osborne, J., and Haines, A.B., "The Interaction between Local Effects at the Shock and Rear Separation – A Source of Significant Scale Effects in Wing-Tunnel Tests on Aerofoils and Wings," AGARD CP 35 (Sep 1968).

6. Pearcey, H.H., and Osborne, J., "Some Problems and Features of Transonic Aerodynamics," 7th Congress of the International Council of the Aeronautical Sciences, Rome, Italy, ICAS Paper 70–14 (Sep 1970).

7. MacCormack, R.W., "Numerical Solution of the Interaction of a Shock Wave with a Laminar Boundary Layer," Lecture Notes in Physics, Vol. 8, Springer Verlag (1971) pp. 151–163.

8. Klineberg, J.M., and Steger, J.L., "Calculation of Separated Flows at Subsonic and Transonic Speeds," July 1972, Proceedings of the 3rd International Conference on Numerical Methods in Fluid Mechanics, Vol. II, Springer-Verlag Berlin (1973) pp. 161–168.

9. Brilliant, H.M., and Adamson, T.C., Jr., "Shock-Wave-Boundary Layer Interactions in Laminar Transonic Flow," AIAA Journal, Vol. 12, pp. 323–329 (Mar 1974).

10. Tai, T.C., "Transonic Laminar Viscous-Inviscid Interaction over Airfoils," AIAA Journal, Vol. 13, No. 8, pp. 1065–1072 (Aug 1975). Also as NSRDC Rpt. 4362 (Jun 1974).

11. Enseki, F.K., "A Calculative Method for the Turbulent Transonic Viscous-Inviscid Interaction on Airfoils," AIAA Paper 72–5, San Diego, Calif. (Jan 1972).

12. Kuhn, G.D., and Nielsen, J.N., "Prediction of Turbulent Separated Boundary Layers," AIAA Paper 73–663, Palm Springs, Calif. (Jul 1973).

13. Melnik, R.E., and Grossman, B., "Analysis of the Interaction of a Weak Normal Shock Wave with a Turbulent Boundary Layer," AIAA Paper 74–598, Palo Alto, Calif. (1974).

14. Mason, W.H., and Inger, G.R., "Analytic Investigation of Transonic Normal Shock-Turbulent Boundary Layer Interaction," VPI-Aero-027, Virginia Polytechnic Institute and State Univ., Blacksburg, Va. (Nov 1974).

15. Tai, T.C., "Transonic Turbulent Viscous-Inviscid Interactions," AIAA Paper 75–78, Pasadena, Calif. (Jan 1975). Also as DTNSRDC Rpt. 4662 (Jan 1976).

16. Deiwert, G.S., "Computation of Separated Transonic Turbulent Flows," AIAA Journal, Vol. 14 (Jun 1976) pp. 735–740.

17. Adamson, T.C., Jr., and Messiter, A.F., "Normal Shock Wave-Turbulent Boundary Layer Interactions in Transonic Flow Near Separation," in *Transonic Flow Problems in Turbomachinery*, edited by Adamson and Platzer, Hermisphere, Washington (1977) pp. 392–414.

18. Gliebe, P.R., "Coupled Inviscid/Boundary Layer Flow Field and Predictions for Transonic Turbomachinery Cascades," in *Transonic Flow Problems in Turbomachinery*, edited by Adamson and Platzer, Hermisphere, Washington (1977) pp. 434–453.

19. Chapman, D.R., "Dryden Lecture: Computational Aerodynamics Development and Outlook," AIAA Journal 17, No. 12, pp. 1293–1313 (Dec 1979).

20. Emmons, H.W., "Flow of a Compressible Fluid past a Symmetrical Airfoil in a Wind Tunnel and Free Air," NACA TN 1746 (Nov 1948).

21. Murman, E.M., and Cole, J.D., "Calculation of Plane Steady Transonic Flows," AIAA Journal, Vol. 9, No. 1, pp. 114–121 (Jan 1971).

22. Murman, E.M., "Analysis of Embedded Shock Waves Calculated by Relaxation Methods," AIAA Journal, Vol. 12, No. 5, pp. 626–632 (1974).

23. Garabedian, P., and Korn, D., "Analysis of Transonic Airfoils," Comm. of Pure and Appl. Math., Vol. 24, pp. 841–851 (1971).

24. Jameson, A., "Transonic Flow Calculations for Airfoils and Bodies of Revolution," Grumman Aerospace Corporation, Bethpage, N.Y., Report 390-71-1 (1971).

25. Jameson, A., "Transonic Potential Flow Calculations using Conservative Form," Proceedings of AIAA 2nd Computational Fluid Dynamics Conference, pp. 148–161 (1975).

26. Martin, E., "A Fast Semi-Direct Method for Computing Transonic Aerodynamic Flows," Proceedings of AIAA 2nd Computational Fluid Dynamics Conference, pp. 162–174 (1975).

27. Hafex, M.M., and Cheng, H.K., "Convergence Acceleration and Shock Fitting for Transonic Flow Computations," Univ. of Southern Calif., Los Angeles, Calif., Report USCAE-132 (1975).

28. Yu, N.J., and Rubbert, P.E., "Acceleration Schemes for Transonic Potential Flow Calculations," AIAA Paper 80-0338, Pasadena, Calif. (Jan 1980).

29. Yoshihara, H., "Some Recent Developments in Planar Inviscid Transonic Airfoil Theory," AGARD AG-156 (Feb 1972).

30. Bailey, F.R., "On the Computation of Two- and Three-Dimensional Steady Transonic Flows by Relaxation Methods," Lecture Notes in Physics, Vol. 19, Springer-Verlag, (1972) pp. 2–9.

31. Jameson, A., "Numerical Computation of Transonic Flows with Shock Waves," in Symposium Transonic II, Springer-Verlag (1976) pp. 384–414.

32. Murman, E.M., "Computation of Transonic Potential Flows in Turbomachinery," in *Transonic Flow Problems in Turbomachinery*, edited by Adamson and Platzer, Hermisphere, Washington, D.C. (1976) pp. 115–138.

33. Ballhaus, W.F., "Some Recent Progress in Transonic Flow Computations," presented at the lecture series on Computational Fluid Dynamics, von Karman Institute for Fluid Dynamics, Belgium (Mar 1976).

34. Bauer, F., Garabedian, P., Korn, D., and Jameson, A., "Supercritical Wing Sections II," Springer-Verlag, New York (1975).

35. Carlson, L.A., "Transonic Airfoil Flowfield Analysis Using Cartesian Coordinates," NASA CR-2577 (Aug 1975).

36. Euvrard, D., and Morchoisne, Y., "Supercritical Flows past Airfoils at Mach Numbers Close to One," Rapport de Recherche 054, Ecole Nationale Superieure de Techniques Avancees, Paris (Sep 1975).

37. Albone, C.M., "A Finite-Difference Scheme for Computing Supercritical Flows in Arbitrary Coordinate Systems," TR 74-90, Royal Aircraft Establishment, Farnborough, England (Sep 1974).

38. Tai, T.C., "Comment on Analysis of Embedded Shock Waves Calculated by Relaxation Methods," AIAA Journal, Vol. 12, No. 5, pp. 735–736 (May 1974).

39. Holt, M., and Masson, B.S., "The Calculation of High Subsonic Flow Past Bodies by The Method of Integral Relations," Proceedings of the Second International Conference on Numerical Methods in Fluid Dynamics, Vol. 8, Springer-Verlag, New York (1971) pp. 207-214.

40. Melnik, R.E., and Ives, D.C., "Subcritical Flows of Two-Dimensional Airfoils by a Multistrip Method of Integral Relations," Proceedings of the Second International Conference on Numerical Methods in Fluid Dynamics, Vol. 8, Springer-Verlag, New York (1971) pp. 243-251.

41. Sato, J., "Application of Dorodnitsyn's Technique to Compressible Two-Dimensional Airfoil Theories at Transonic Speeds," National Aerospace Lab., Tokyo, Japan, Report TR-220T (Oct 1970).

42. Tai, T.C., "Transonic Inviscid Flow over Lifting Airfoils by the Method of Integral Relations," AIAA Journal, Vol. 12, No. 6, pp. 798–804 (Jun 1974). Also as NSRDC Rpt 3424, (Jul 1972).

43. Holt, M., "A Review of Numerical Techniques for Calculating Supercritical Airfoil-Flows," Symposium Transsonicum II, Springer-Verlag, New York (1975) pp. 362–368.

44. Magnus, R., and Yoshihara, H., "Inviscid Transonic Flow over Airfoils," AIAA Journal, Vol. 8, No. 12, pp. 2157–2162 (Dec 1970).

45. Stivers, L.S., Jr., "Effects of Subsonic Mach Numbers on the Forces and Pressure Distributions on Four NACA 64A–Series Airfoil Section at Angles of Attach as High as 28°," NACA TN 3162 (Mar 1954).

46. Garabedian, P.R., and Korn, D.G., "Numerical Design of Transonic Airfoils," Numerical Solution of Partial Differential Equations, Vol. 2, Academic Press, New York (1971) pp. 253–271.

47. Krupp, J.A., and Murman, E.M., "Computation of Transonic Flows Past Lifting Airfoils and Slender Bodies," AIAA Journal, Vol. 10, No. 7, pp. 880–886 (Jul 1972).

48. Kacprzynski, J.J., Ohman, L.H., Garabedian, P.R., and Korn, D.G., "Analysis of the Flow Past a Shockless Lifting Airfoil in Design and Off-Design Conditions," National Research Council of Canada, Ottawa, Canada, Aero Rept. LR-544 (Nov 1971).

49. Liepmann, H.W., and Roshko, A., "Elements of Gas Dynamics," Wiley, New York (1957).

50. Chan, S.T.K., and Brashears, M.R., "Finite Element Analysis of Transonic Flow," AFFDL Technical Report AFFDL-TR-74-11 (Mar 1974).

51. Hafez, M.M., Wellford, L.C., Merkle, C.L., and Murman, E.M., "Numerical Computation of Transonic Flows by Finite-Element and Finite-Difference Methods," NASA CR-3070 (Dec 1978).

52. Tijdeman, H., and Schippers, P., "Results of Pressure Measurements on an Airfoil with Oscillating Flap in Two-Dimensional High Subsonic and Transonic Flow," NLR-TR 73078, (1973).

53. Oswatitsch, K., "Die Geschwindigkeitsverteilung an Symmetrischen Profilen beim Augtreten Lokaler Überschallgebiete," Acta Physica Austriaca, Vol. 4, pp. 228–271 (1951).

54. Gullstrand, T.R., "Transonic Flow Past Two-Dimensional Aerofoils," Zeitsschrift für Flugwissenshaften, Vol. 1, pp. 28–46 (1953).

55. Spreiter, J.R., and Alksne, A., "Theoretical Prediction of Pressure Distributions on Nonlifting Airfoils at High Subsonic Speeds," NACA Report 1217 (1955).

56. Norstrud, H., "Numerische Lösungen für Schallnahe Strömungen um Ebene Profile," Zeitschrift für Flugwissenschaften, Vol. 18, pp. 149–157 (1970).

57. Nixon, D., "Extended Integral Equation Method for Transonic Flows," AIAA Journal, Vol. 13, pp. 934–935 (Jul 1975).

58. Nixon, D., "Calculation of Transonic Flows Using an Extended Integral Equation Method," AIAA Journal, Vol. 15, No. 3, pp. 295–296 (Mar 1977).

59. Klineberg, J.M., and Lees, L., "Theory of Laminar Viscous-Inviscid Interactions in Supersonic Flow," AIAA Journal, Vol. 17, pp. 2211–2221 (Dec 1969).

60. Stewartson, K., "Correlated Incompressible and Compressible Boundary Layers," Proceedings of the Royal Society: Ser. A, Mathematical and Physical Sciences, Vol. 200, pp. 85-100 (1949).

61. Klineberg, J.M., Kubota, T., and Lees, L., "Theory of Exhaust-Plume/Boundary-Layer Interactions at Supersonic Speeds," AIAA Journal, Vol. 10, pp. 581–588 (May 1972).

62. Coles, D., "The Law of the Wake in the Turbulent Boundary Layer," Journal of Fluid Mechanics, Vol. 1 (1956).

63. Kleinstein, G., "Generalized Law of the Wall and Eddy-Viscosity Model for Wall Boundary Layers," AIAA Journal, Vol. 5, No. 8, pp. 1402–1407 (Aug 1967).

64. Klebanoff, P.S., "Characteristics of Turbulence in a Boundary Layer with Zero Pressure Gradient," NACA Report 1247 (1955).

65. Alber, I.E., "Similar Solutions for a Family of Separated Turbulent Boundary Layers," AIAA Paper 71–203, New York (Jan 1971).

66. Alber, I.E., Bacon, J.W., Masson, B.S., and Collins, D.J., "An Experimental Investigation of Turbulent Transonic Viscous-Inviscid Interactions," AIAA Journal, Vol. II, No. 5, pp. 620–627 (May 1973).

67. Nash, J.F., and Macdonald, A.G.J., "The Calculation of Momentum Thickness in a Turbulent Boundary Layer at Mach Numbers up to Unity," Aeronautical Research Council, London, C.P. Report 963 (1967).

68. Head, M.R., "Entrainment in the Turbulent Boundary Layer," Aeronautical Research Council, London, R. and M. Report 3152 (Sep 1958).

69. McDonald, H., and Stoddart, J.A.P., "On the Development of the Incompressible Turbulent Boundary Layer," Aeronautical Research Council, London, R. and M. Report 3484 (Mar 1965).

70. Bradshaw, P., Ferriss, D.H., and Atwell, N.P., "Calculation of Boundary-Layer Development Using the Turbulent Energy Equation," Aeronautical Research Council, London, NPL Aero Report 1182, 27 667 (Jan 1966).

71. Schubauer, E.B., and Spangenberg, W.G., "Forced Mixing in Boundary Layers," Journal of Fluid Mechanics, Vol. 8, Part 1, pp. 10–32 (May 1960).

72. Stratford, B.S., and Beavers, G.S., "The Calculation of the Compressible Turbulent Boundary Layer in an Arbitrary Pressure Gradient – A Correlation of Certain Previous Methods," Aeronautical Research Council, London, R. and M. Report 3207, (1961).

73. Lees, L., and Reeves, B.L., "Supersonic Separated and Reattached Laminar Flows: I. General Theory and Application of Adiabatic Boundary Layer Shock Wave Interactions," AIAA Journal, Vol. 2, pp. 1907–1920 (Nov 1964).

74. Oswatitsch, K., "Die Ablösungsbedingung von Grenzschichten," Symposium of Boundary Layer Research, edited by H. Görtler, Springer-Verlag, Berlin, Germany (1958) pp. 357–367.

75. Chapman, D.R., Kuehn, D.M., and Larson, H.K., "Investigation of Separated Flows in Supersonic and Subsonic Streams with Emphasis on the Effect of Transition," NACA Report 1356 (1958).

76. Lighthill, M.J., "On Displacement Thickness," Journal of Fluid Mechanics, pp. 383-392 (Aug 1958).

77. Schubauer, G.B. "Air Flow in a Separating Laminar Boundary Layer," NACA Report 527 (1935).

78. Collins, D.J., and Krupp, J.A., "Experimental and Theoretical Investigations in Two-Dimensional Transonic Flow," AIAA Journal, Vol. 12, pp. 771–778 (Jun 1974).

79. Murman, E.M., "Computation of Wall Effects in Ventilated Transonic Wind Tunnels," AIAA Paper 72–1007, Palo Alto, Calif. (1972).

80. Graham, D.J., Nitzbery, G.E., and Olson, R.N., "A Systematic Investigation of Pressure Distribution at High Speeds over Five Representative NACA Low-Drag and Conventional Aerofoil Sections," NACA Report 832 (1945).

81. Lees, L., and Reeves, B.L., "Some Remarks on Integral Moment Methods for Laminar Boundary Layers with Application to Separation and Reattachment," Firestone Flight Science Lab., Calif. Inst. of Tech., Pasadena, Calif., Technical Report (Dec 1961).

82. Ferrari, C., and Tricomi, F.G., "Transonic Aerodynamics," translated by R.H. Cramer, Academic Press, New York (1968) pp. 586–589.

83. Schlichting, H., "Boundary Layer Theory," 6th English Edition, McGraw-Hill, New York (1968) p. 600.

84. Kerrebrock, J.L., "Dryden Lectureship in Research-Flow in Transonic Compressors," AIAA Paper 80–0124, Pasadena, Calif. (Jan 1980).

85. Vavra, M.H., "Aero-Thermodynamics and Flow in Turbomachines," Wiley, New York (1960).

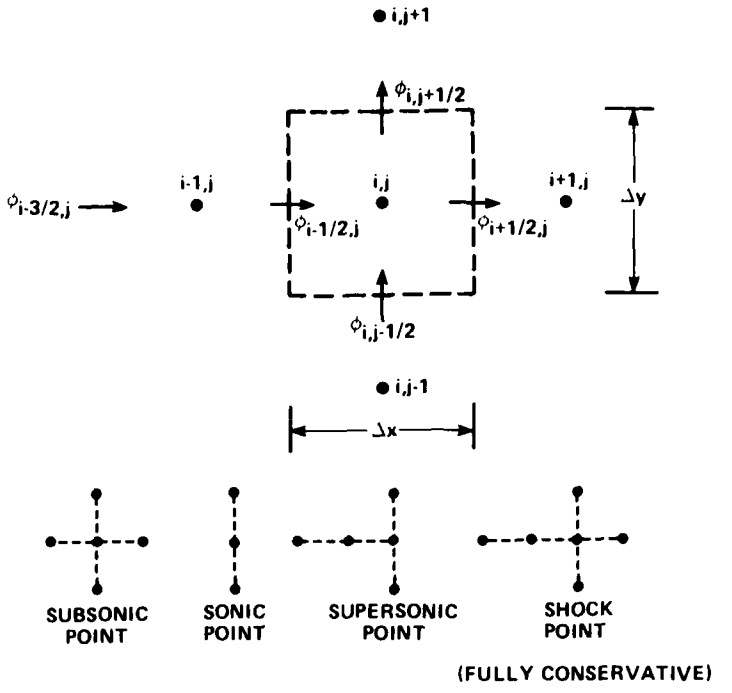

Figure 1 – Mesh System for the Finite Difference Method
(Illustration is based on Ref. 32)

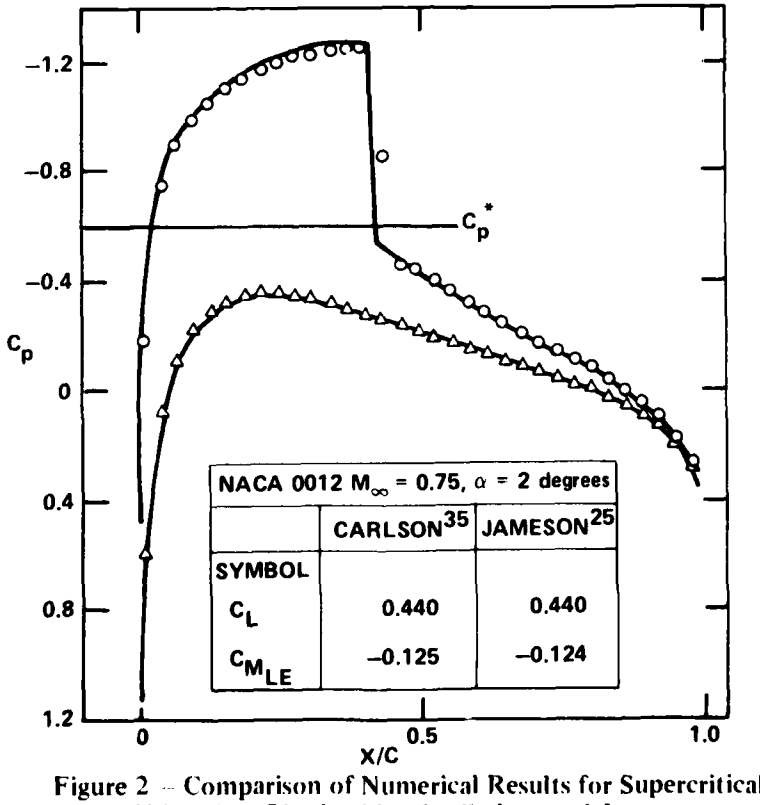

Figure 2 – Comparison of Numerical Results for Supercritical Lifting Case Obtained by the Carlson and Jameson Finite Difference Codes

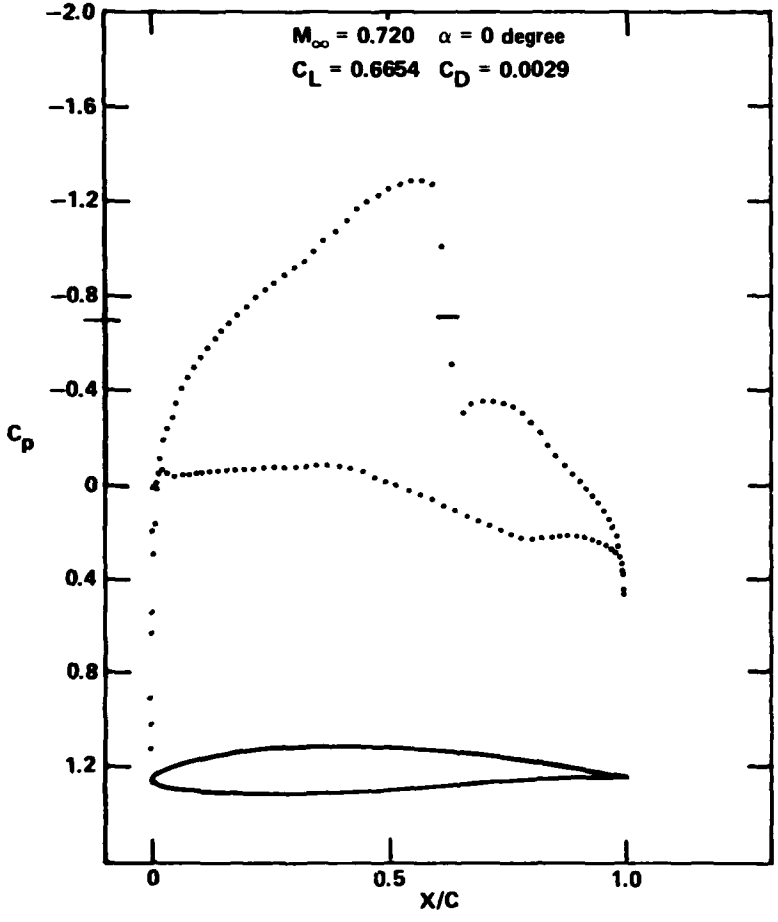

Figure 3a – Conservative Difference

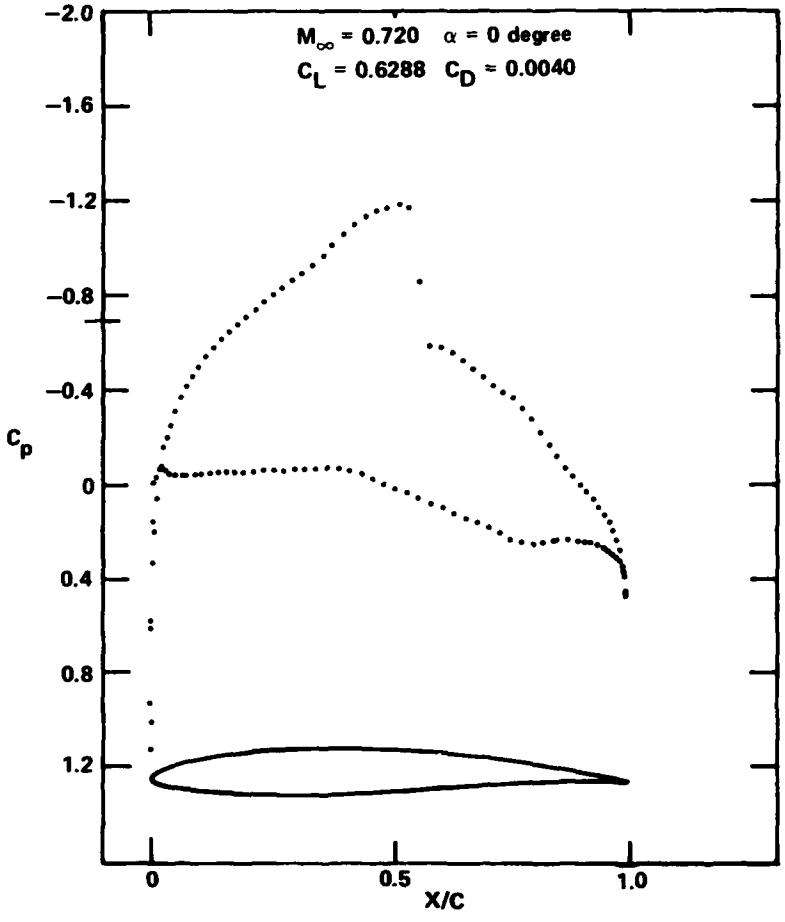

Figure 3b – Nonconservative Difference

Figure 3 – Comparison of Numerical Results Using Conservative versus Nonconservative Difference Forms for the Potential-Flow Solution for Flow Past an NACA 64A410 Airfoil
(Illustration is based on Ref. 32)

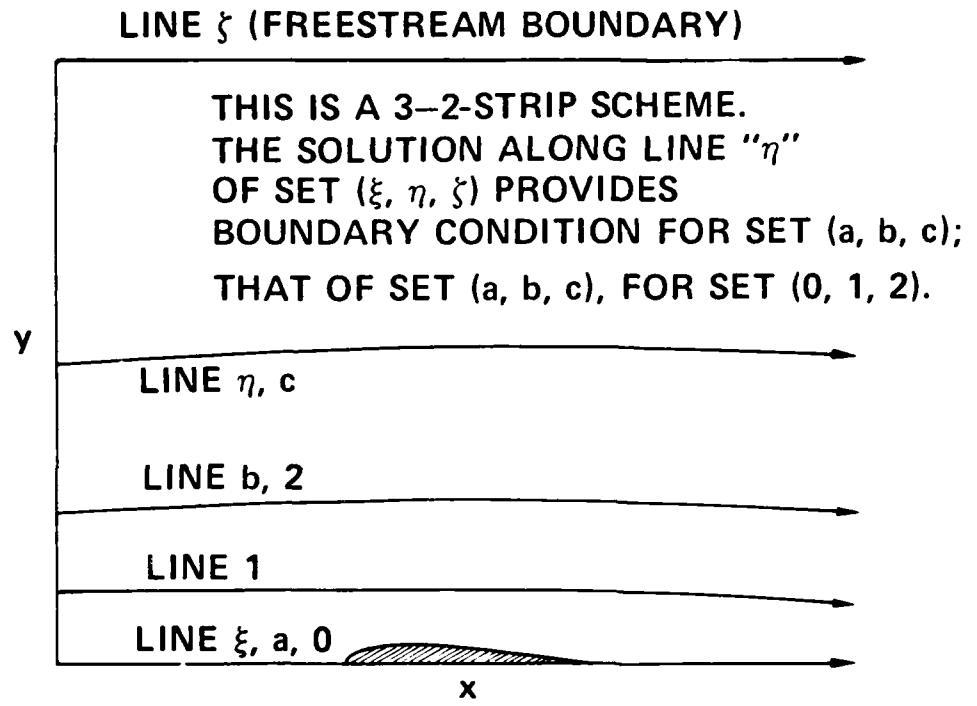

Figure 4 – Extension of Freestream Boundary to "Infinity" for Flowfield Solved by the Method of Integral Relations

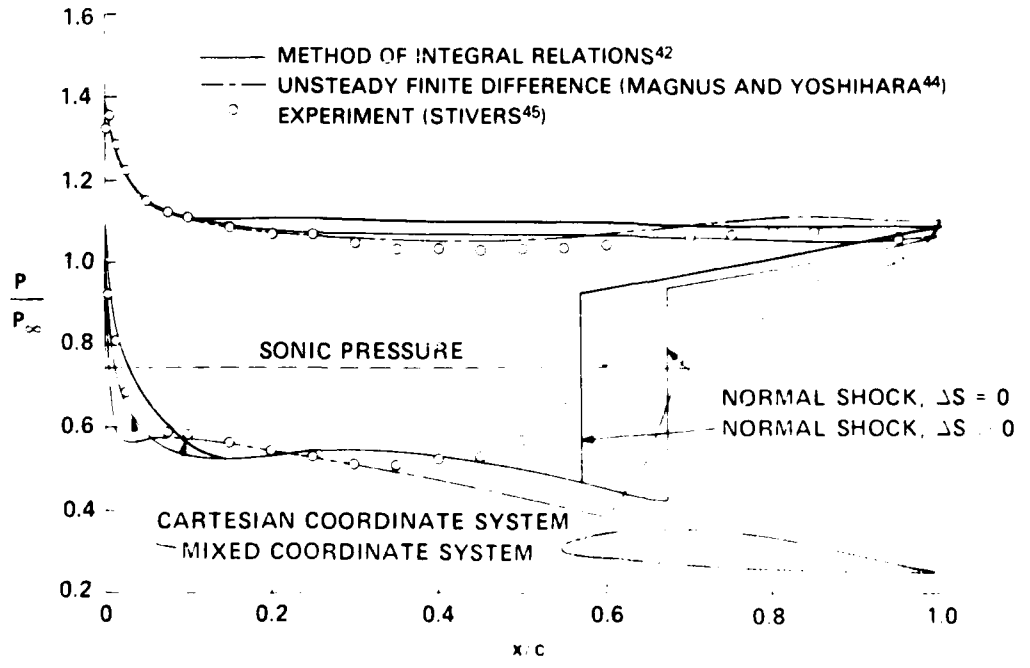

Figure 5 Pressure Distribution on an NACA 64A410 Airfoil at $M_\infty = 0.72$ and $\alpha = 4$

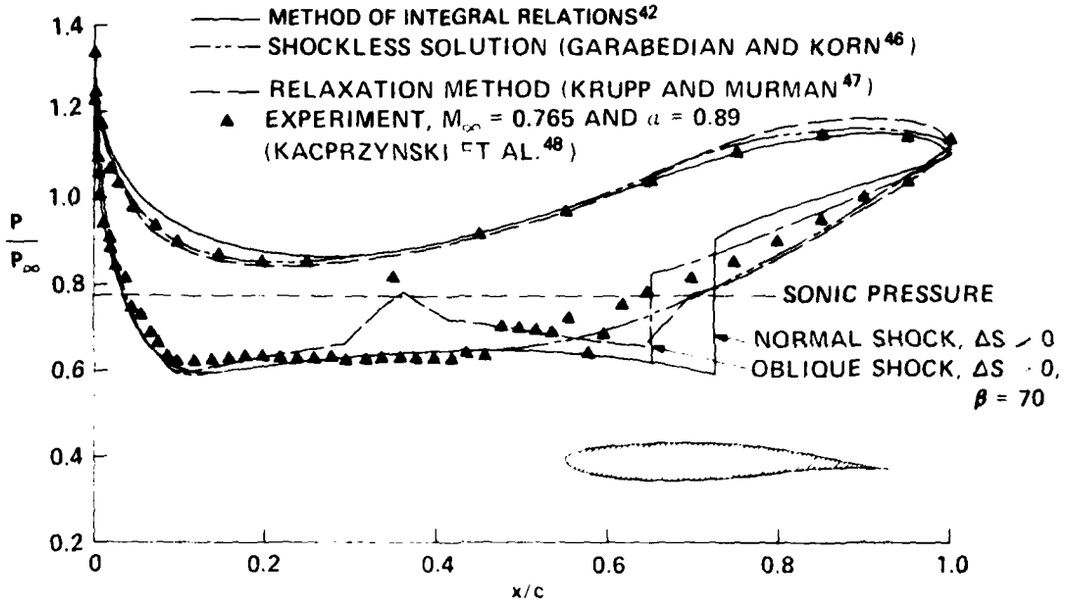

Figure 6 – Pressure Distribution on a Garabedian-Korn Airfoil at $M_\infty = 0.75$

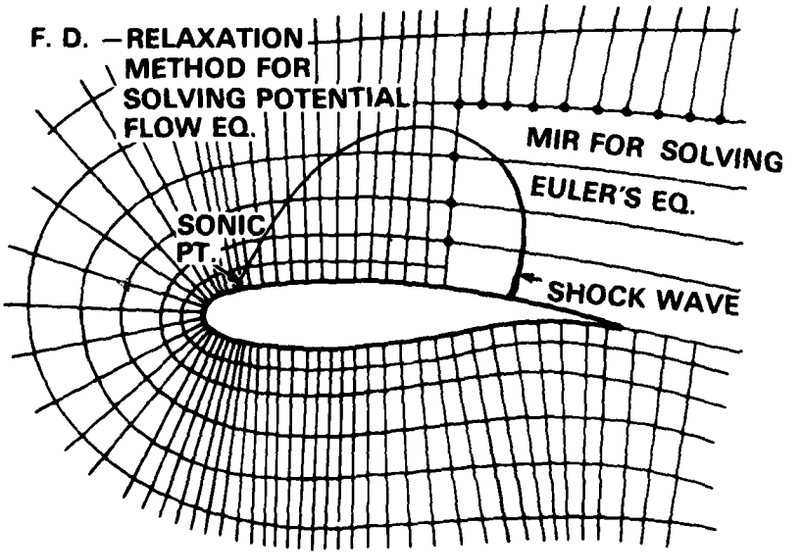

Figure 7 – Hybrid Method (Finite Difference Method Embedded With the Method of Integral Relations) for Solving Transonic Flow With Moderate and Strong Shock Waves

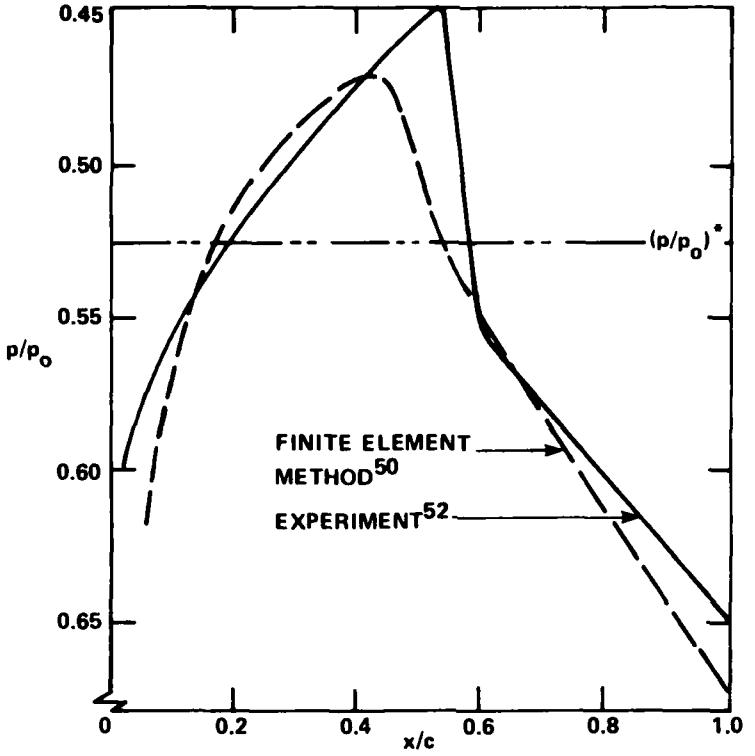

Figure 8 – Pressure Distribution Over an NACA 64A006 Airfoil at $\alpha = 0$ *degree and* $M_\infty = 0.875$ *Calculated by the Finite Element Method*

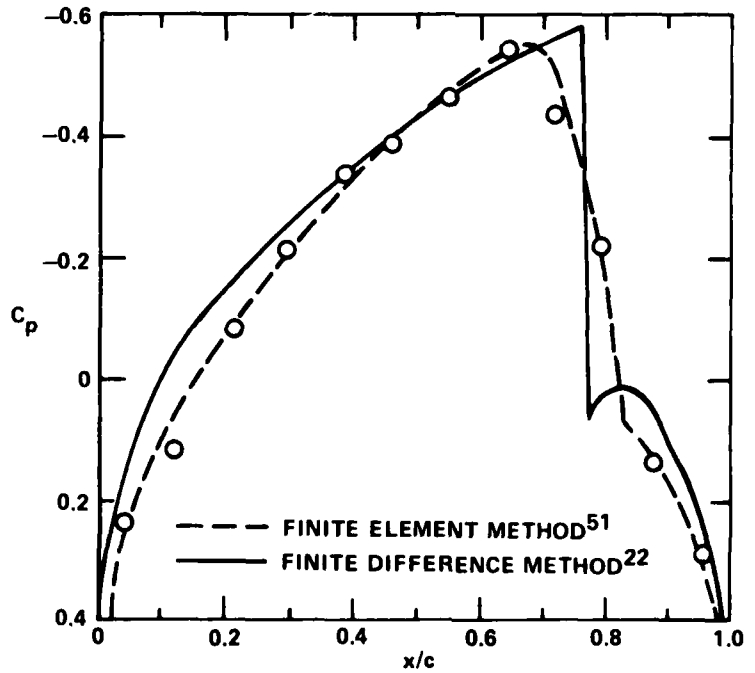

Figure 9 – Comparison Between the Numerical Results Obtained by the Finite Element Method and the Finite Difference Method for Transonic Small Disturbance Equation

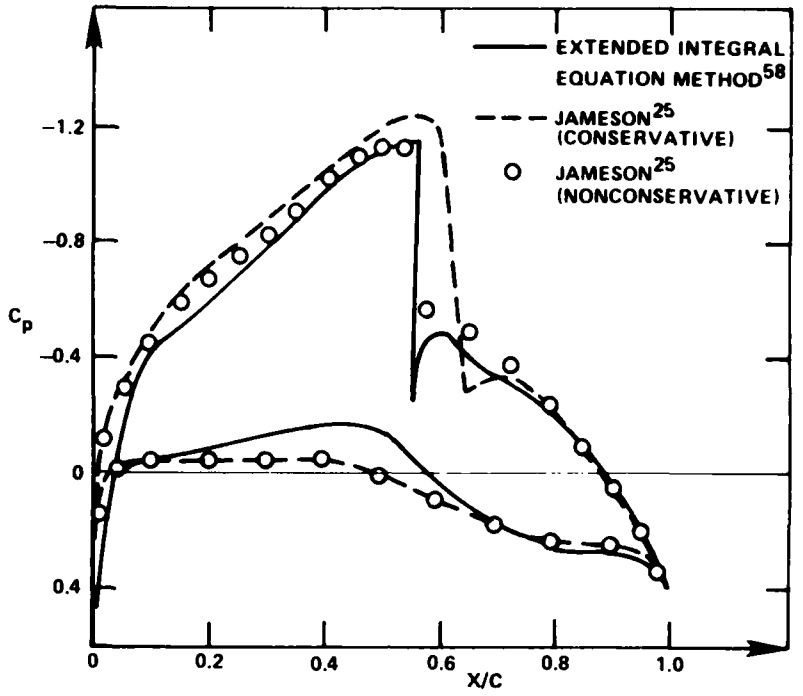

Figure 10 – Theoretical Pressure Distributions Around an NACA 64A410 Airfoil at $M_\infty = 0.72$, and $\alpha = 0$ Degrees
(Illustration based on Ref. 58)

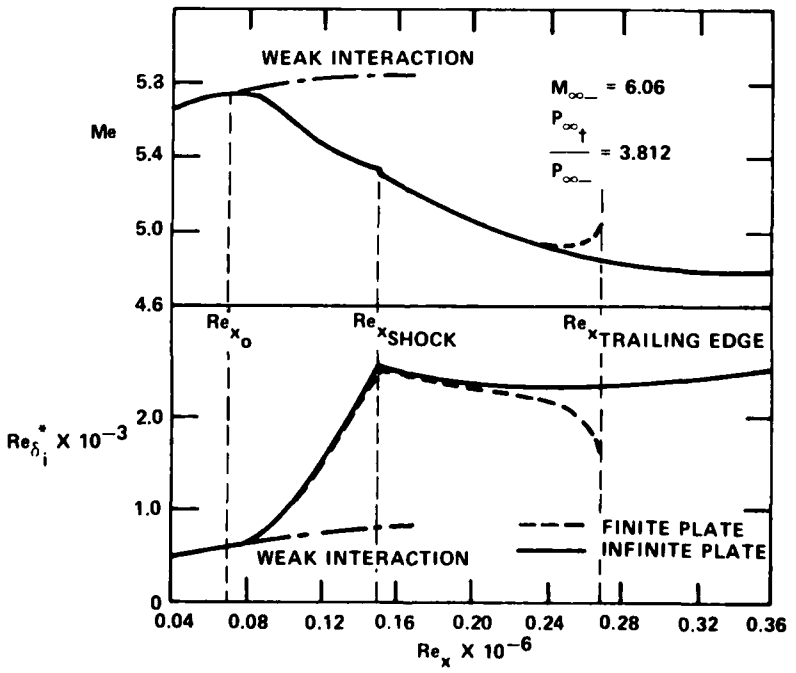

Figure 11 – Results of Adiabatic Laminar Boundary-Layer Shock-Wave Interaction by the Klineberg-Lees Method Over Flat Plate at Supersonic Speed
(Illustration based on Ref. 59)

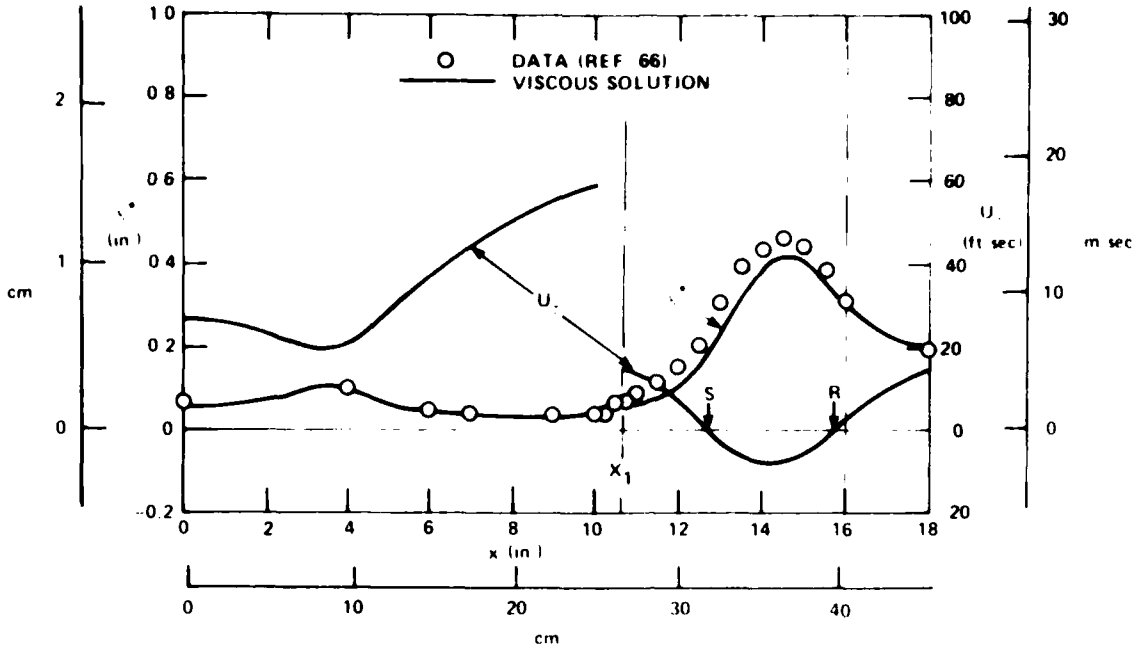

Figure 12 Results of an Adiabatic Turbulent Boundary Layer Flow Past a Bump at Transonic Speed by Kuhn-Nielsen Method
(Illustration based on Ref. 12)

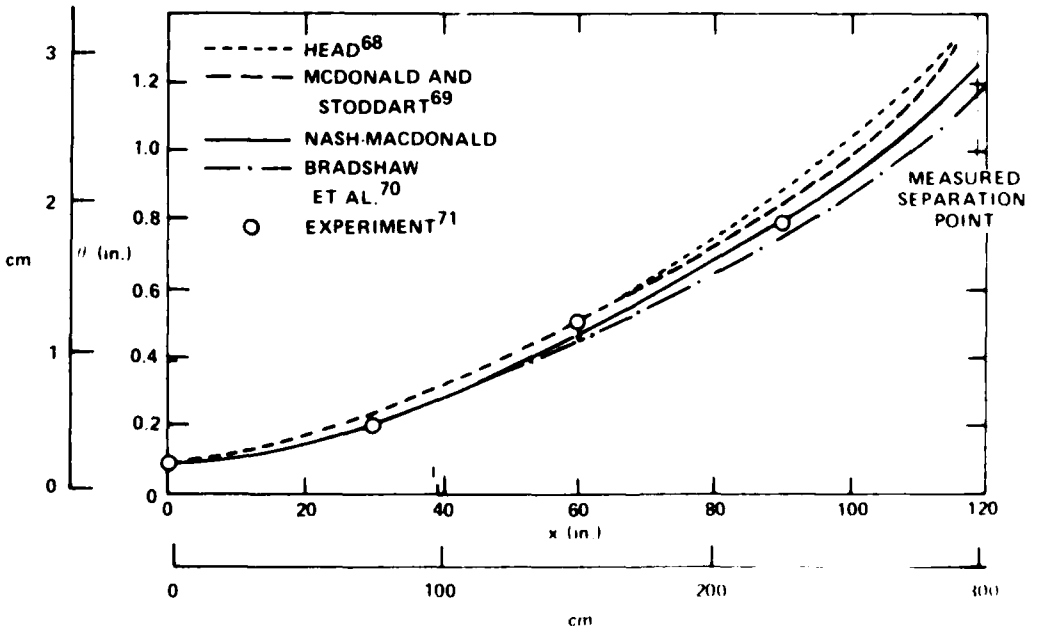

Figure 13 Momentum Thickness of a Compressible Turbulent Boundary Layer Calculated by Nash-Macdonald Method Together with Others

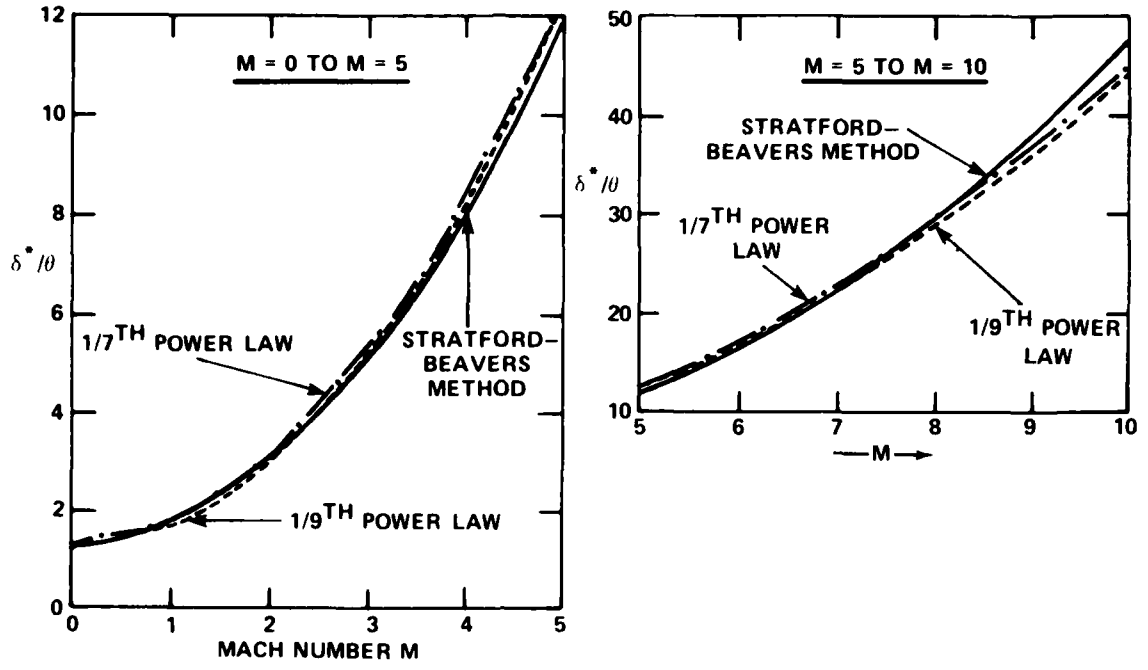

Figure 14 - Profile Shape Parameter δ^*/θ of a Compressible Turbulent Boundary Layer Calculated by Stratford-Beavers Method

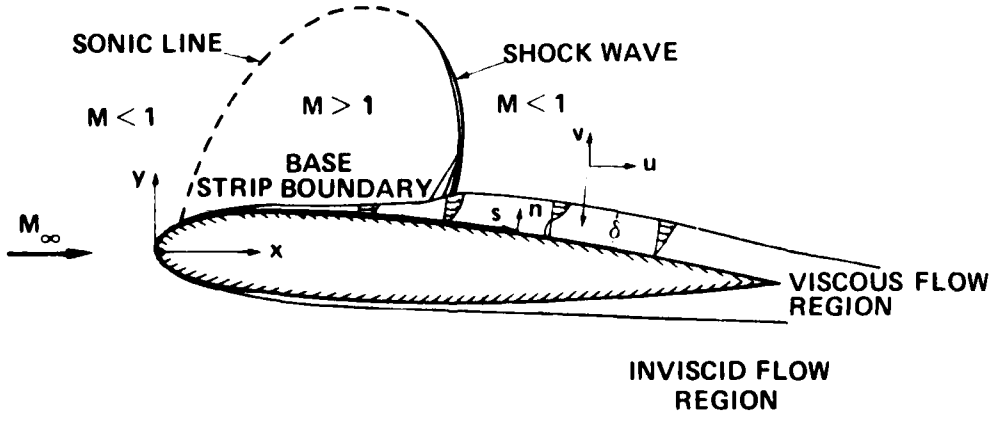

Figure 15 Transonic Viscous-Inviscid Interaction Over an Airfoil

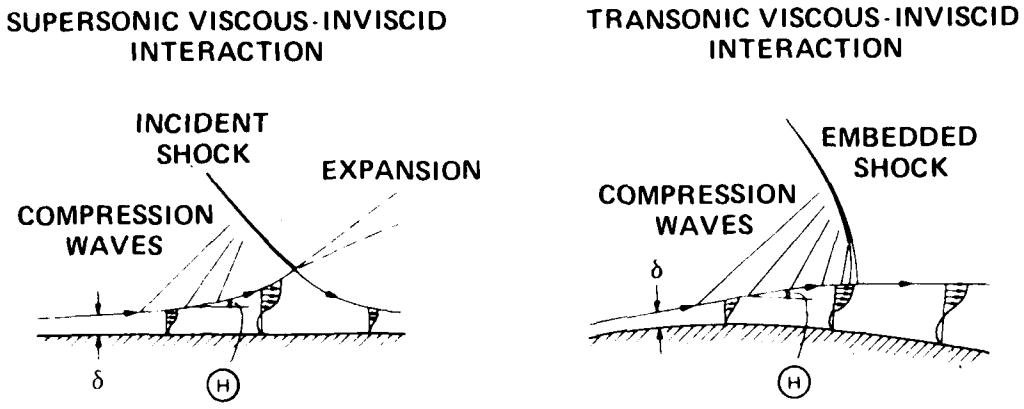

Figure 16 – Schematic of Supersonic and Transonic Viscous-Inviscid Interactions

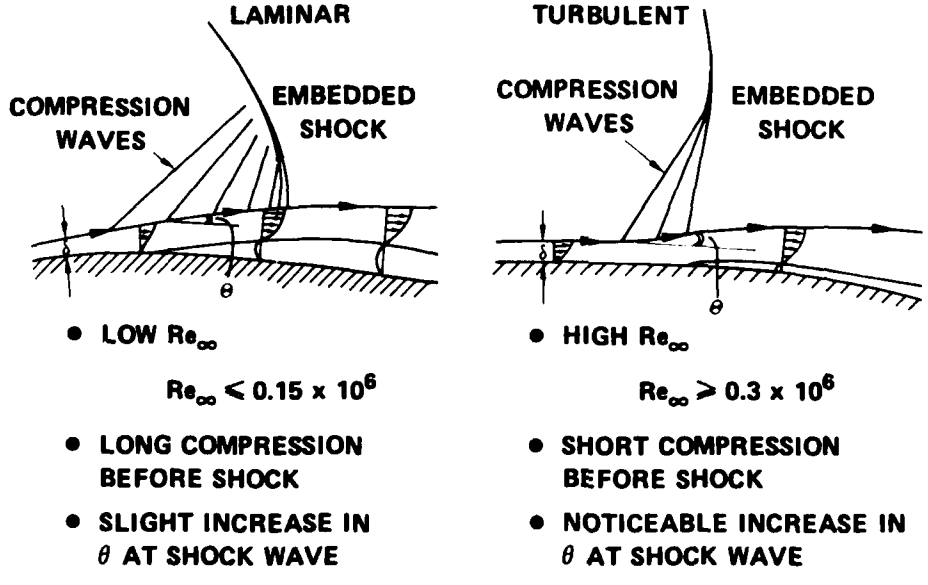

Figure 17 – Comparison of Laminar and Turbulent Viscous-Inviscid Interactions

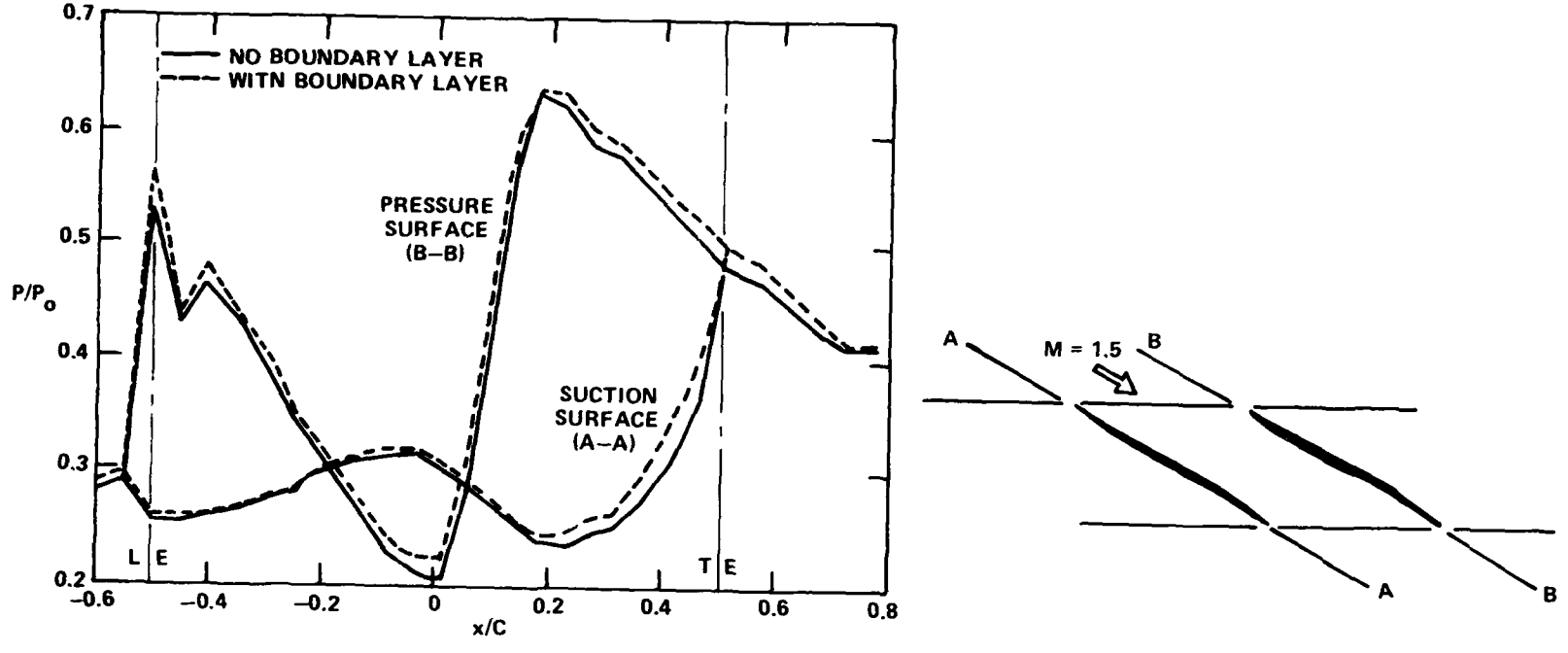

Figure 18 – Effect of Boundary Layer on Blade Surface Pressures in a Transonic Fan Rotor Tip Section Cascade
(Illustration based on Ref. 18)

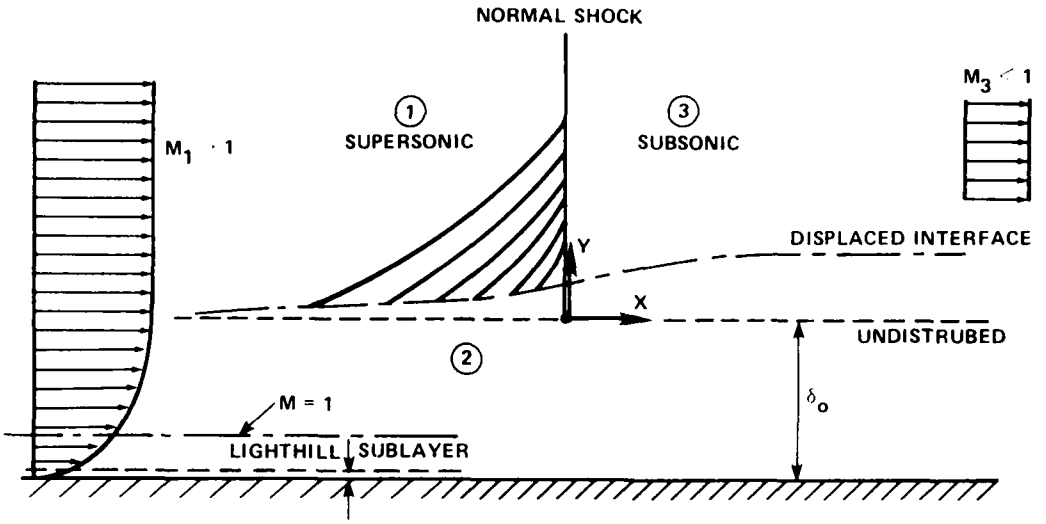

Figure 19 Schematic of Flow Model for Analytical Investigation of Transonic Viscous-Inviscid Flow Used by Manson and Inger

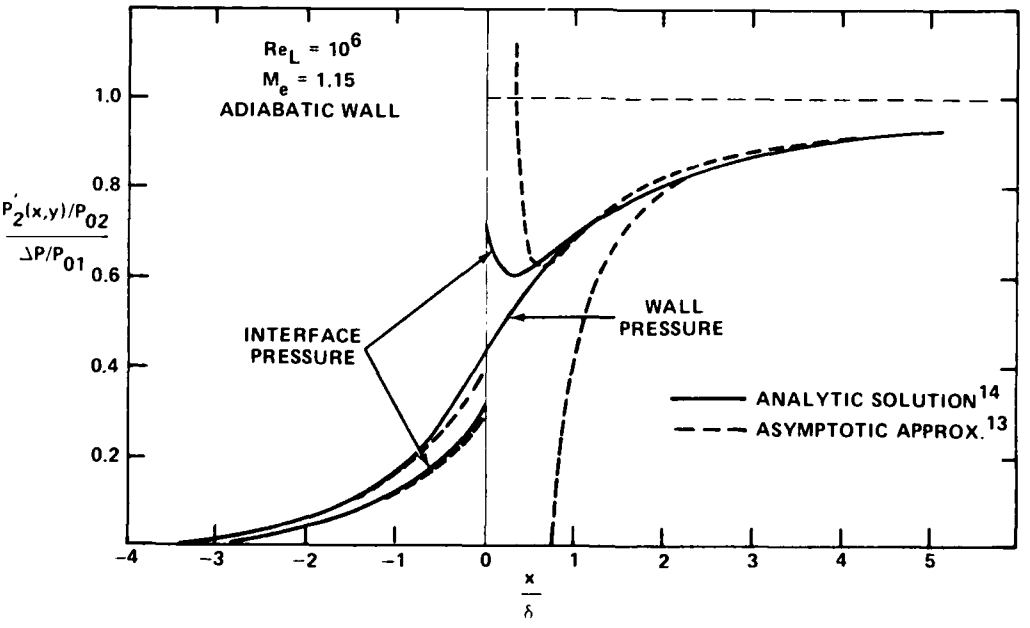

Figure 20 Comparison of Results Obtained by Analytical Solution and Asymptotic Approximation

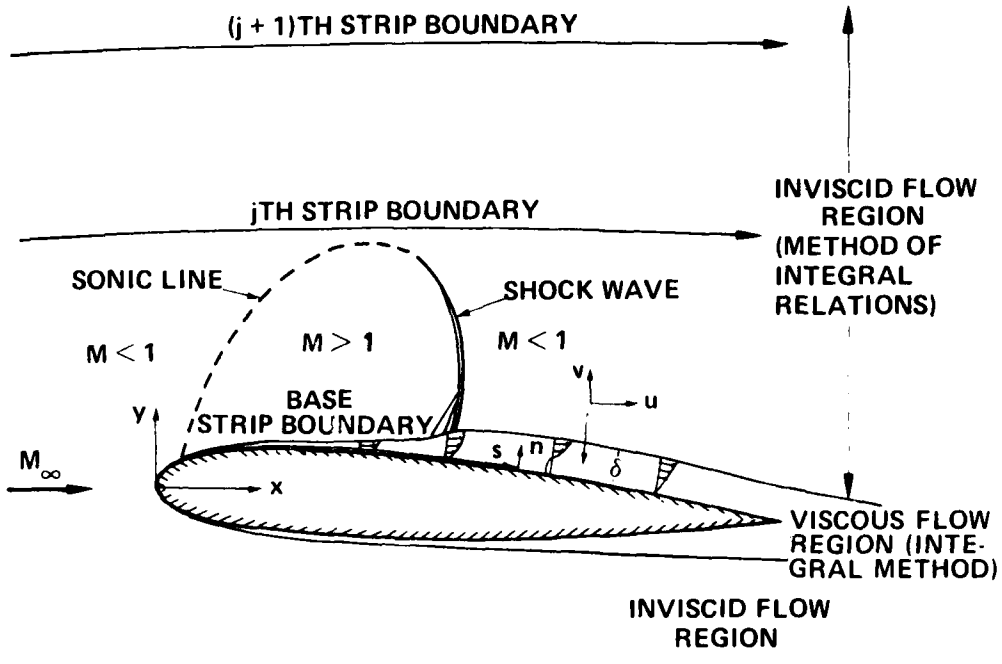

Figure 21 – Coordinate Systems and Flow Regions for Calculation of Viscous-Inviscid Transonic Flow

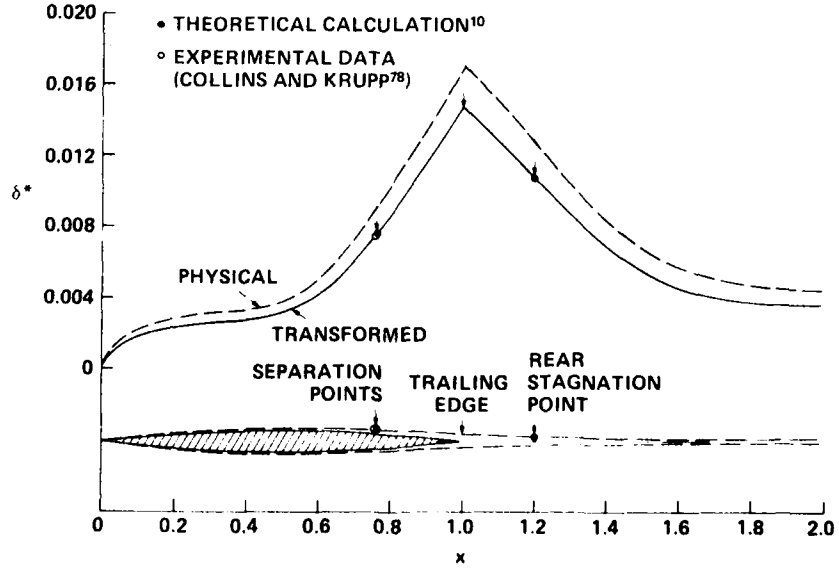

Figure 22 – Boundary-Layer Displacement Thickness for a 6% Circular Arc at $M_\infty = 0.868$ and $Re_\infty = 6.9 \times 10^4$

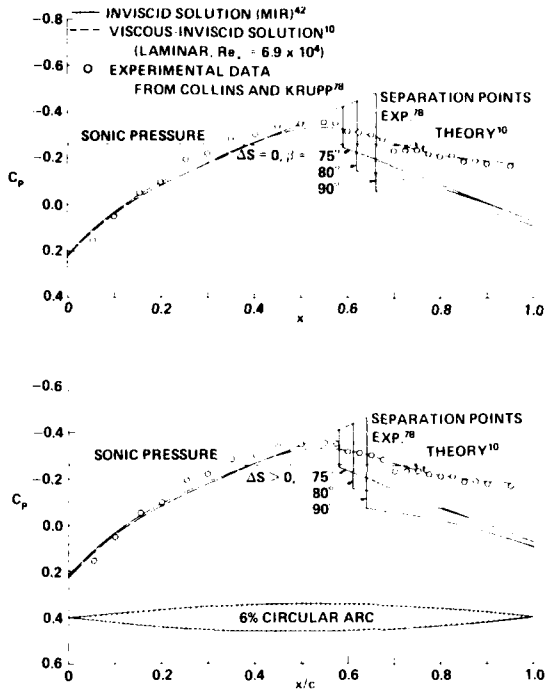

Figure 23 – Pressure Distribution Over a 6% Circular Arc at $M_\infty = 0.868$ and $\alpha = 0°$

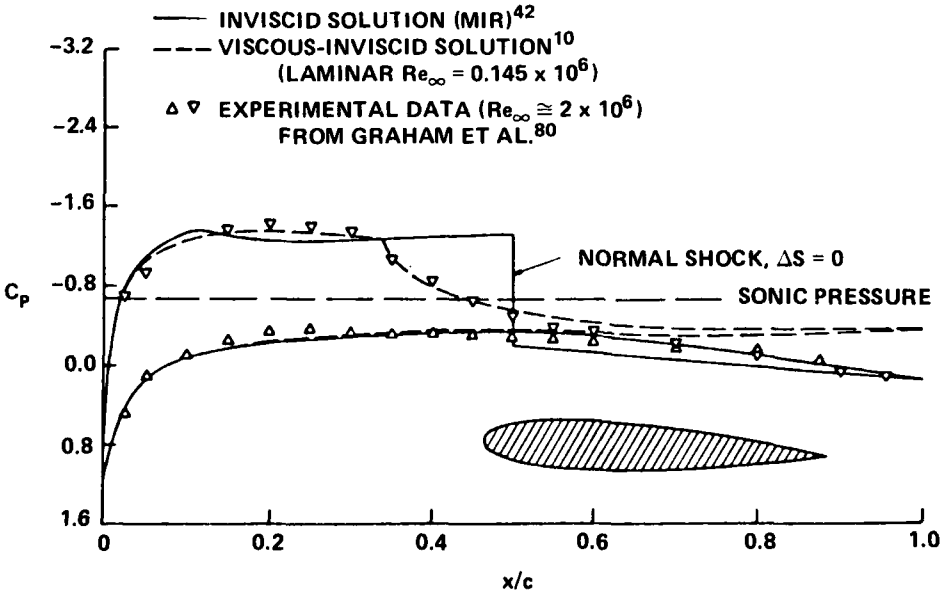

Figure 24 – Pressure Distribution on an NACA 0015 Airfoil at $M_\infty = 0.729$ and $\alpha = 4°$

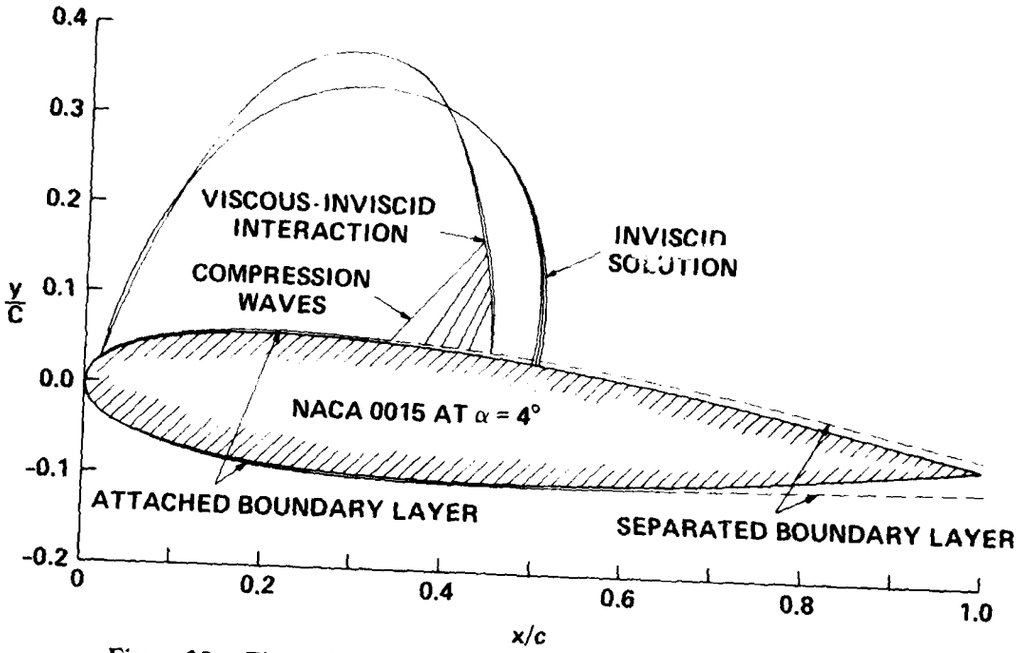

Figure 25 – Flowfield of a NACA 0015 Airfoil at $M_\infty = 0.729$, $\alpha = 4°$, and $Re_\infty = 0.145 \times 10^6$

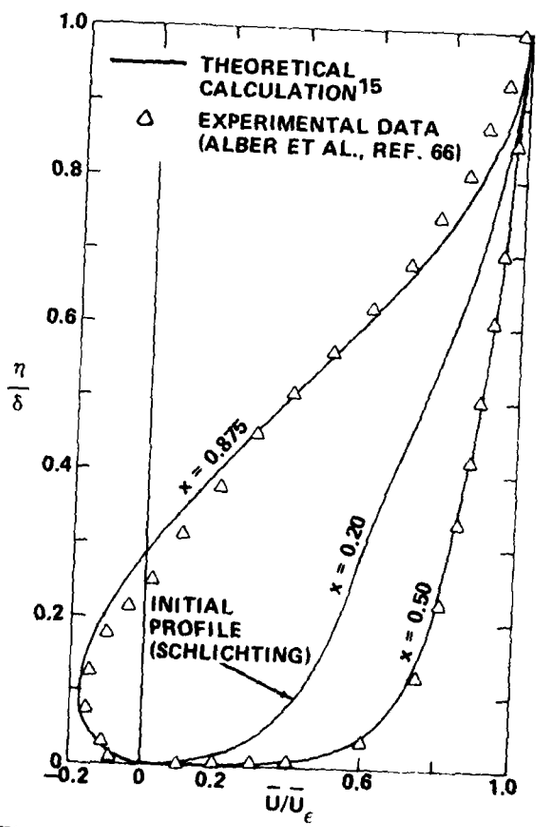

Figure 26 – Turbulent Boundary Layer-Velocity Profiles on a 10% Thickness Bump at $M_\infty = 0.7325$

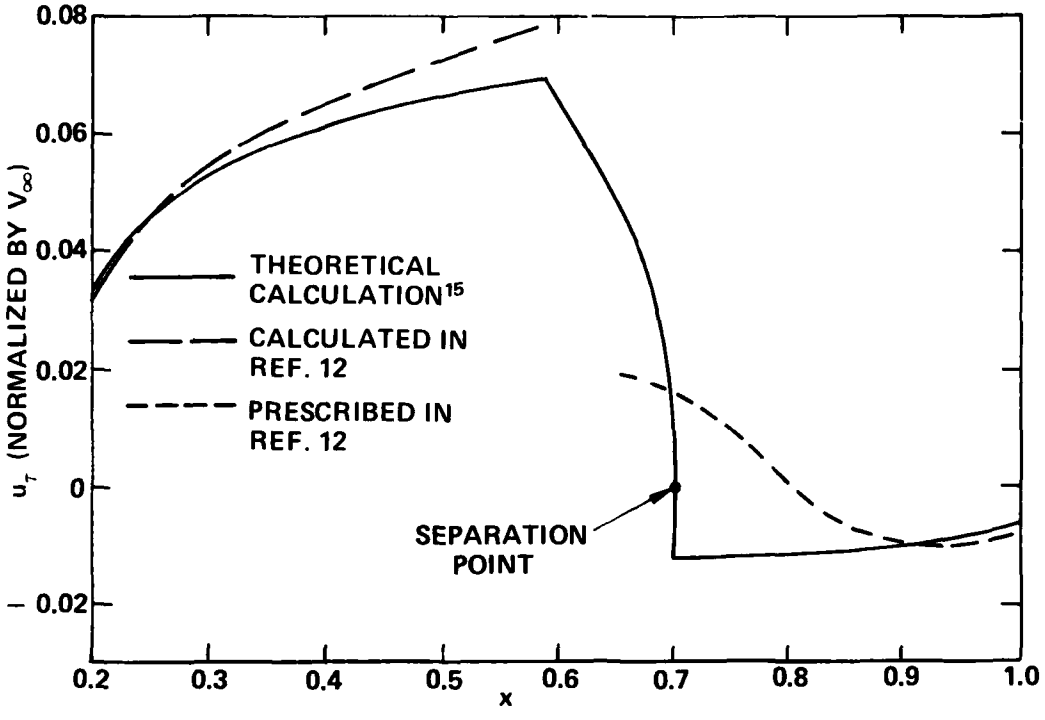

Figure 27 – Calculated Friction-Velocity Distribution Over a 10% Thickness Bump at $M_\infty = 0.7325$

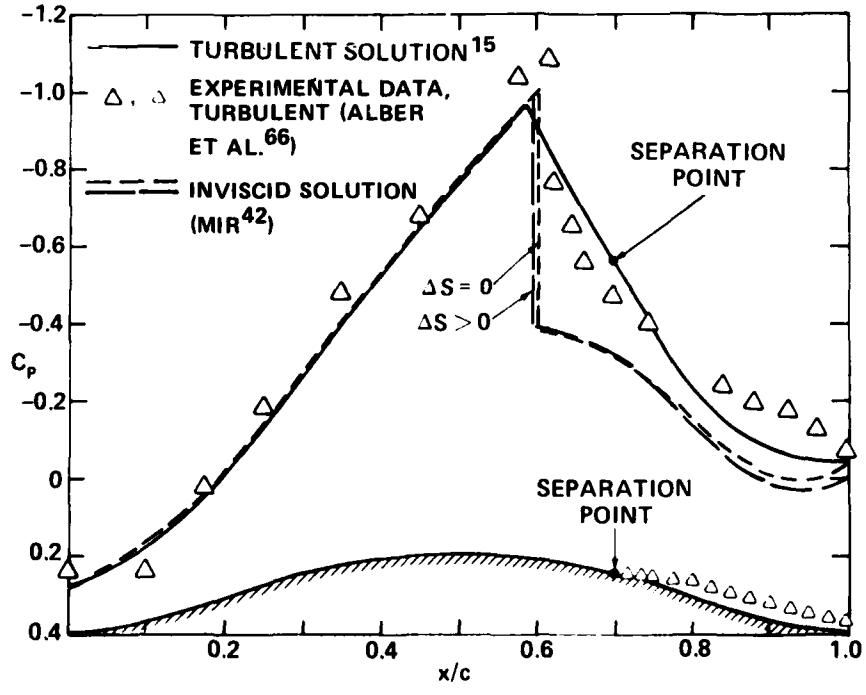

Figure 28 – Pressure Distribution Over a 10% Thickness Bump at $M_\infty = 0.7325$ and $Re_\infty = 1.75 \times 10^6$

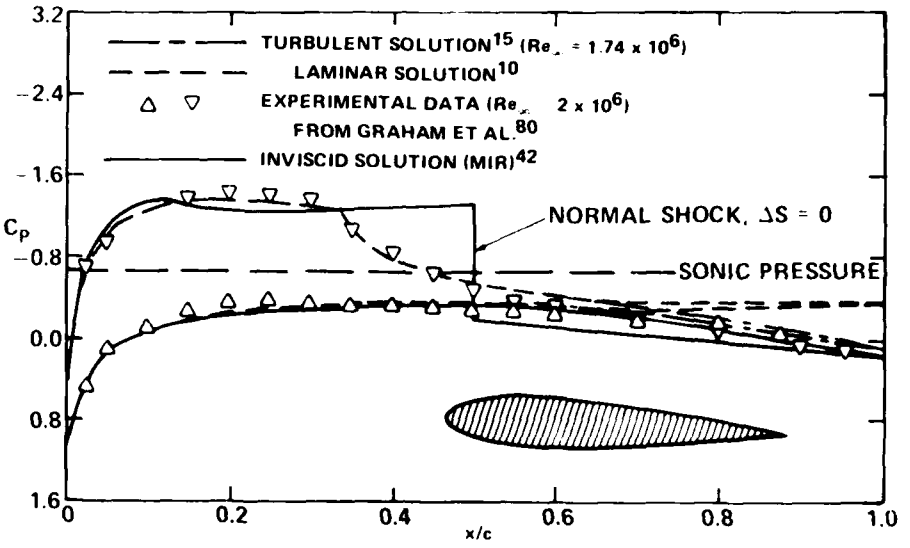

Figure 29 – Pressure Distribution on an NACA 0015 Airfoil at $M_\infty = 0.729$ and $\alpha = 4$ Degrees

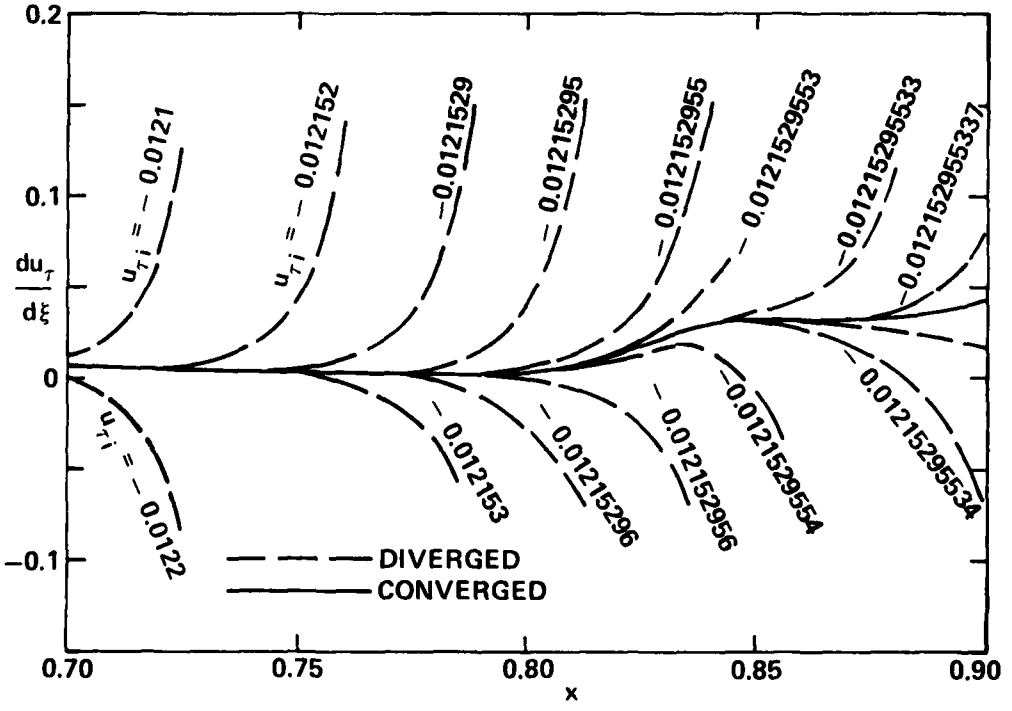

Figure 30 – Friction Velocity Gradients Downstream of the Separation Point (Ref. 15)

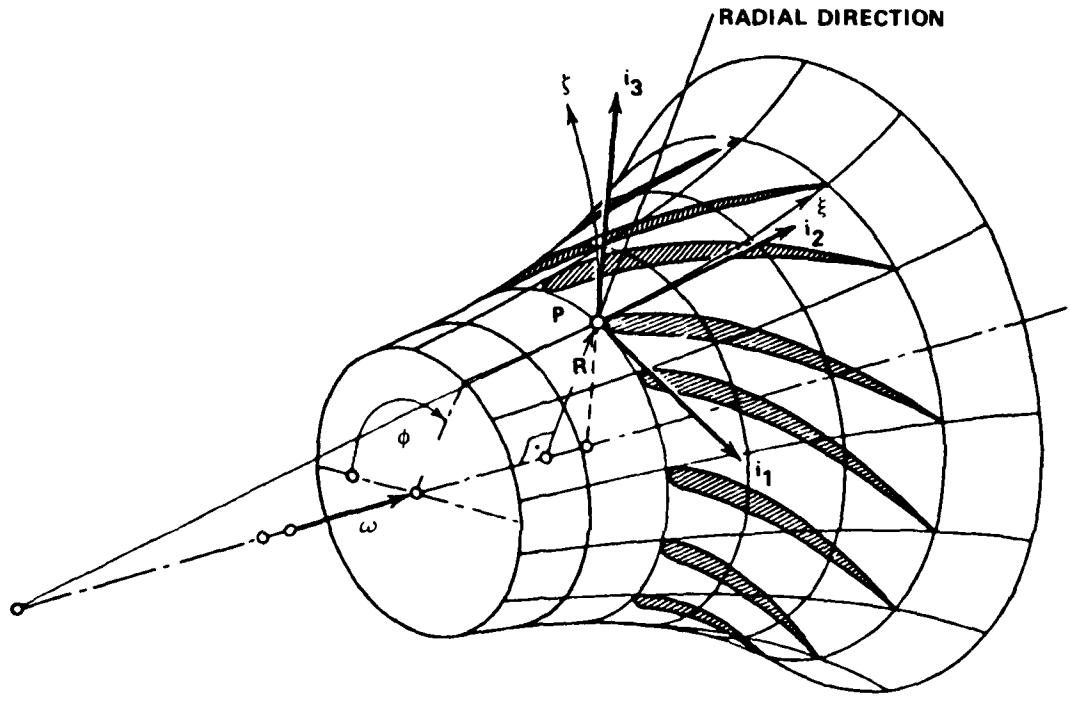

Figure 31 – Quasi Two-Dimensional Flow on Axisymmetric Stream Surface
(Illustration based on Ref. 85)

INITIAL DISTRIBUTION

Copies	
2	DDR&E
	1 Lib
	1 R.F. Siewert (OAD/ET)
4	CNR
	1 211
	1 430B
	1 432
	1 438
4	ONR
	1 ONR Boston
	1 ONR Chicago
	1 ONR London, England
	1 ONR Pasadena
1	NRL
1	USNA
5	NAVPGSCOL
	1 Lib
	1 L. Schmidt
	1 M. Platzer
	1 G.N. Vanderplaats
	1 D.J. Collins
4	NADC
	1 Lib
	1 W.A. Langan
	1 K.T. Yen
	1 C. Mazza
5	NWC/China Lake
	1 W.H. Clark
	1 C.F. Markarian
	1 R. van Aken
	1 R.E. Meeker
	1 Lib
2	NSWC/Dahlgren
	1 F.G. Moore
	1 Lib
3	NSWC/White Oak
	1 Lib
	1 T.F. Zien
	1 L.H. Schindel

Copies	
18	NAVAIRSYSCOM
	1 AIR 03A
	1 AIR 03C
	1 AIR 03E
	1 AIR 03PA
	1 AIR 03PA3
	1 AIR 310
	1 AIR 320
	3 AIR 320D
	1 AIR 5105
	1 AIR 530B
	4 AIR 5301
	1 AIR 950D
	1 PMA 269
5	NAVSEASYSCOM
	1 SEA 03B
	1 SEA 031
	1 SEA 032
	1 SEA 033
	1 SEA 09G32
1	NAVAIRPROPTESTCEN
3	PMTC
	1 Lib
	1 J.W. Rom
	1 A.A. Anderson
12	DTIC
1	AFOSR
2	USAFA
	1 Lib
	1 R.W. Gallington
1	AF INST TECH
2	AFFDL
	1 Lib
	1 W. Hankey
1	AEDC

Copies		Copies	
8	NASA	2	Clemson U
	1 HQ, Washington, D.C.		1 Lib
	3 Ames Research Center		1 T. Yang/Mech Engr Dept
	1 Lib		
	1 R. Presley	1	U. of Colorado
	1 G.H. Kidwell		
	3 Langley Research Center	1	Cornell U
	1 Lib		
	1 R. Margason	1	U. of Delaware
	1 J. South		
	1 Lewis Research Center	2	Georgia Inst Tech
			1 Lib
1	U of Akron		1 Aerospace Engr
1	U of Alabama	1	Harvard U
1	U. Arizona	1	Howard U
1	Boston U.	1	Illinois Inst Tech
1	Brown U/Div of Engr	1	U. of Illinois
1	Brooklyn Polytech.	1	Iowa S.U.
2	Calif Inst of Tech	1	Johns Hopkins U
	1 Grad Aero Labs		
	1 T. Kubota	3	APL/Johns Hopkins U
			1 Lib
1	Calif Inst of Tech/Jet Prop Lab		1 L.L. Cronvich
			1 L.B. Weckesser
2	U of Calif/Berkeley		
	1 Lib	1	U of Kentucky
	1 M. Holt/Div Aero Sciences		
		1	Louisiana S.U.
1	U of Calif/L.A.		
		4	U of Maryland
1	U of Calif/LaJolla		1 Lib
			1 Aerospace Engr
2	U of S. Calif		1 J.D. Anderson, Jr.
	1 Lib		1 S.I. Pai
	1 H.K. Cheng		
		1	MIT
1	Catholic U of America		
		2	U of Michigan
1	Case Western Reserve U.		1 Lib
			1 Aerospace Engr
2	U of Cincinnati		
	1 Lib	1	Michigan S.U.
	1 Aerospace Engr		

Copies		Copies	
1	Mississippi S.U.	1	G. Washington U.
1	New York U/Courant Inst Math Sci	1	W. Virginia U/Dept Aero Engr
1	U of N. Carolina	1	U of Wisconsin
2	N. Carolina State U/Raleigh 1 Lib 1 F.R. DeJarnette/Mech & Aerospace Engr	1	American Inst of Aeronautics & Astronautics
		1	Advanced Tech Ctr
1	Notre Dame U.	1	ARO Inc
1	Ohio State U.	1	ARAP/Princeton, N.J.
1	Pennsylvania State U	1	AVCO-Everett Res. Lab/Everett MA
1	Princeton U	1	Bell Aerospace
1	Purdue U	1	Boeing Company/Seattle
1	Rensselaer Polytech	1	Boeing Aerospace Co/Seattle
1	Rutgers State U.	1	Calspan Corp/Buffalo, NY
2	San Deigo State College 1 Lib 1 K.C. Wang/Mech Engr	2	Douglas Aircraft/Long Beach, CA 1 Lib 1 T. Cebeci
1	Stanford U	1	Fairchild-Republic Corp/ Farmingdale, NY
1	Stevens Inst Tech	1	Flow Research/Kent Washington
2	U of Tennessee Space Inst 1 Lib 1 C.M. Wu	1	General Dynamics/Convair
		1	General Dynamics/Fort Worth
1	Texas A & M U.	1	Grumman Aerospace Corp
1	U of Toledo	1	Hughes Aircraft Co
1	U of Virginia/Alderman Lib	1	Inst for Defense Analyses
3	Virginia Polytech Inst 1 Carol M. Newman Lib 1 Aero & Ocean Engr 1 G.R. Inger	1	Kaman Corp/Bloomfield, Conn.
		1	Lockheed-California
1	U of Washington	1	Lockheed-Georgia

Copies	
1	Lockheed Missiles & Space Co
1	LTV Aerospace Corp
1	Martin Marietta Labs/Baltimore, MD
2	McDonnell Douglas/St. Louis 1 MCAIR 1 MDRL
1	Nielsen Engr & Res Inc
1	Northrop Corp/Hawthorne, CA
1	Rockwell International Corp/ Columbus, Ohio
1	Sandia Laboratories/Albuquerque
1	The Marquardt Co/Van Nuys, CA
1	TRW Systems Group
1	United Technology/East Hartford, Conn.
1	Vought Corp

CENTER DISTRIBUTION

Copies	Code	Name
1	28	
10	5211.1	Reports Distribution
1	522.1	Lib (C)
1	522.2	Lib (A)
2	522.3	Aero Lib

Copies	Code	Name
5	012	
1	11	
1	15	
1	1562	
1	16	
1	166	
1	18	
1	1840	
1	1843	
1	27	

DTNSRDC ISSUES THREE TYPES OF REPORTS

1. DTNSRDC REPORTS, A FORMAL SERIES, CONTAIN INFORMATION OF PERMANENT TECHNICAL VALUE. THEY CARRY A CONSECUTIVE NUMERICAL IDENTIFICATION REGARDLESS OF THEIR CLASSIFICATION OR THE ORIGINATING DEPARTMENT.

2. DEPARTMENTAL REPORTS, A SEMIFORMAL SERIES, CONTAIN INFORMATION OF A PRELIMINARY, TEMPORARY, OR PROPRIETARY NATURE OR OF LIMITED INTEREST OR SIGNIFICANCE. THEY CARRY A DEPARTMENTAL ALPHANUMERICAL IDENTIFICATION.

3. TECHNICAL MEMORANDA, AN INFORMAL SERIES, CONTAIN TECHNICAL DOCUMENTATION OF LIMITED USE AND INTEREST. THEY ARE PRIMARILY WORKING PAPERS INTENDED FOR INTERNAL USE. THEY CARRY AN IDENTIFYING NUMBER WHICH INDICATES THEIR TYPE AND THE NUMERICAL CODE OF THE ORIGINATING DEPARTMENT. ANY DISTRIBUTION OUTSIDE DTNSRDC MUST BE APPROVED BY THE HEAD OF THE ORIGINATING DEPARTMENT ON A CASE-BY-CASE BASIS.


ATE
LME